Available online at www.sciencedirect.com

SciVerse ScienceDirect

Procedia Engineering 00 (2012) 000–000

Procedia Engineering

www.elsevier.com/locate/procedia

5th BSME International Conference on Thermal Engineering

Thermal conductivity, viscosity and density of R141b refrigerant based nanofluid

I.M. Mahbubul[a]*, R. Saidur[a,b], M.A. Amalina[a]

[a]*Department of Mechanical Engineering, University of Malaya, 50603 Kuala Lumpur, Malaysia*
[b]*UM Power Energy Dedicated Advanced Centre (UMPEDAC), Level 4, Wisma R&D, University of Malaya, 59990 Kuala Lumpur, Malaysia*

Abstract

Nanofluids attract researchers in many ways for its enhanced heat transfer properties. Nanorefrigerant is one kind of nanofluids. It has better heat transfer performance than traditional refrigerants. Recently, some experiments have been done about nanorefrigerant, which are mostly related to heat transfer performance of these fluids. Thermal conductivity, viscosity and density are the basic thermophysical properties that must be analyzed before performance analysis. In this paper, the volumetric effects of thermal conductivity, viscosity and density of Al_2O_3/R141b nanorefrigerant have been studied for different temperature ranges. Based on the analysis about nanorefrigerant it is found that, thermal conductivity increases with the increase of volume concentrations and temperatures. However, viscosity and density increases accordingly with the enhancement of volume concentrations and decreases with the increase of temperature. As, heat transfer performances increases with the augmentation of thermal conductivity and pressure drop and pumping power increases with the enhancement of viscosity and density. Therefore, an optimum volume concentration of nanorefrigerant could improve the performance of a refrigeration system.

Keywords: Nanofluid; Nanorefrigerant; Volume concentration; Temperature.

1. Introduction

In 1995, Stephen Choi [1] introduced the term nanofluid as a promising heat transfer fluid. Nanofluid is a solid-liquid mixture that consists of nanoparticles and a base liquid. Due to very small sizes and large specific surface areas of the nanoparticles, nanofluids have superior properties like high thermal conductivity, minimal clogging in flow passages, long-term stability, and homogeneity [2]. The nanorefrigerant is one kind of nanofluid and its host fluid is refrigerant [3]. Conventional thermo fluids like: ethylene glycol, water, oil and refrigerant have poor heat transfer properties. But these fluids have vast application in power generation, chemical processes, heating and cooling processes, transportation, electronics, automotive and other micro-sized applications. Therefore, re-processing of these thermo fluids for better heat transfer performance is very essential.

Recently (since 2005) scientists are trying to work on nanorefrigerant a kind of nanofluids for its enhance heat transfer performance in refrigeration and air-conditioning systems [3]. Refrigerants are widely used in refrigeration and air conditioning systems in industries, offices, and domestic and commercial buildings. Huge amount of energy is used by this equipment. Nanorefrigerants are potential to enhance heat transfer rate thus making heat exchanger of air conditioning and

* Corresponding author. Tel.: +6 03 7967 7611; fax: +6 03 7967 5317.
E-mail address: mahbub_ipe@yahoo.com

refrigeration equipment compact. This consequently will reduce energy consumption in these sectors along with reduction in emissions, global warming potential and greenhouse gas effects. There are some literatures on the pool boiling, nucleate boiling, and convective heat transfer, energy performance and lubrication of nanorefrigerants. It may be noted that these performance parameters are depend on different thermophysical properties like thermal conductivity, viscosity, and density of a fluid or refrigerant [4-6]. Heat transfer performance is directly related to thermal conductivity of that substance. Viscosity is an important phenomenon as like as thermal conductivity. Pumping power and pressure drop is directly related to viscosity of any fluid, especially in laminar flow. Like the viscosity, density of any fluid is also has direct impact over pressure drop and pumping power characteristics. There are available literatures about thermal conductivity and viscosity of nanofluids [7, 8]. Most of these studies are based on water or ethylene glycol. Nevertheless, literatures about thermophysical properties of refrigerant based nanofluids are still scarce.

The objective of this study is to investigate the thermal conductivity, viscosity and density of Al_2O_3 nanoparticles suspended in R141b refrigerant at different concentrations of nanoparticles and at different temperatures. This study will help the researchers to get the idea about the effect of nanoparticles on the fundamental properties of refrigerant which will encourage the researchers to apply nanoparticles in refrigeration and air conditioning systems. Though, R141b refrigerant is not used in refrigeration and air conditioning system. It is mainly used to produce soft pu foam. However, the fundamental properties of other refrigerants like: R134a, R22, R410 are similar with this refrigerant. Moreover, those refrigerants are in vapor state at atmospheric environment. For this reason nanoparticle could not be mixed with them at open environment to prepare nanorefrigerants.

2. Methodology

2.1. Materials and preparation

Al_2O_3 nanoparticles as manufacturer defined size of 13 nm were purchased from Sigma Aldrich (Malaysia). R141b refrigerant was used as the base fluid as it is liquid at atmospheric pressure and room temperature. Its boiling point is 32.06ºC at atmospheric pressure. The equation that used to calculate the volume fraction of nanorefrigerant was:

$$\varphi = \frac{m_n / \rho_n}{m_n / \rho_n + m_r / \rho_r} \tag{1}$$

Where, φ is the nanoparticle concentration; m_n and m_r are the mass of nanoparticle and refrigerant, respectively; and ρ_n and ρ_r are the density of nanoparticle and liquid phase density of refrigerant, respectively.

Then nanorefrigerant was prepared with an orbital incubator shaker. The mixture of nanoparticles and refrigerant was continuously shaken at 240 rpm about 1 hour. Constant temperature of 15ºC was maintained inside the incubator to avoid evaporation of refrigerant.

2.2. Thermal conductivity of nanorefrigerant

A thermal conductivity model that considered the effects of particle volume fraction, particle size and temperature-dependent interfacial layer proposed by Sitprasert et al. [9] was used to determine the thermal conductivity of Al_2O_3/R141b nanorefrigerant. Other models such as: Maxwell [10], Hamilton-Crosser [11], Yu-Choi [12], Koo-Kleinstreuer [13] and Leong et al. [14] models were used to verify the results of the present study. The thermal conductivity of nanorefrigerant was calculated by,

$$k_{r,n} = \frac{\left(k_p - k_l\right)\phi k_l\left[2\beta_1^3 - \beta^3 + 1\right] + \left(k_p + 2k_l\right)\beta_1^3\left[\phi\beta^3\left(k_l - k_r\right) + k_r\right]}{\beta_1^3\left(k_p + 2k_l\right) - \left(k_p - k_l\right)\phi\left[\beta_1^3 + \beta^3 - 1\right]} \tag{2}$$

Where, $k_{r,n}$, k_p, k_r are the thermal conductivity of nanorefrigerant, solid particles and pure refrigerant, respectively.

$\beta = 1 + \frac{t}{r_p}, \beta_1 = 1 + \frac{t}{2r_p}$; The thickness of interfacial layer, t depends on temperature where $t = 0.01\left(T - 273\right)r_p^{0.35}\Big)$, and the thermal conductivity of the interfacial layer can be found from $k_l = C\frac{t}{r_p}k_r$; where C = 30, a constant for Al_2O_3 nanoparticles, T is the temperature in Kelvin and r_p is the radius of nanoparticles.

2.3. Viscosity of nanorefrigerant

Peng et al. [15] suggested Brinkman model [16] to determine the viscosity of nanorefrigerants. Abedian and Kachanov [17] proved that the model is better than Einstein model [18] when high particle volume fraction is considered. Brinkman model [16] stated as following was used to investigate the viscosity of nanorefrigerant,

$$\mu_{rn} = \mu_r \frac{1}{\left(1-\phi\right)^{2.5}} \tag{3}$$

Where, μ_{rn} is the effective viscosity of nanorefrigerant and μ_r is the viscosity of pure refrigerant.

Other models such as: Einstein [18], Krieger and Dougherty (K-D) [19] and Batchelor [20] models were used to verify the results of the present study

2.4. Density of nanorefrigerant

The density of nanorefrigerant was measured by KEM-DA130N portable density meter (KYOTO, Japan). It measured the density with resonant frequency method. It could measure density within a range of 0.0000 to 2.0000 g/cm^3 with a precision of ±0.001 g/cm^3. It has the resolution of 0.0001 g/cm^3 and can measure density within a temperature range of 0 to 40.0°C. Figure 1 shows the accuracy of the machine. The comparison of the measured data with REFPROP7 [21] standard data base shows maximum deviation is only about 0.2 %. This device was a small and portable type and the inlet tube was very small capillary. High concentration of nanorefrigerants could not support this device. Therefore, very low concentrations of nanorefrigerant were measured. Densities of pure R141b and 0.1 to 0.4 volume % of Al_2O_3/R141b were measured for a temperature range of 5 to 20°C. All the data was taken three times to get more precise values and the mean value of three data was considered for analysis. Some of the data (about 5 %) were omitted as considered abnormality, especially above 20°C. When the refrigerant was evaporated at above 20°C, some of data showed abnormality.

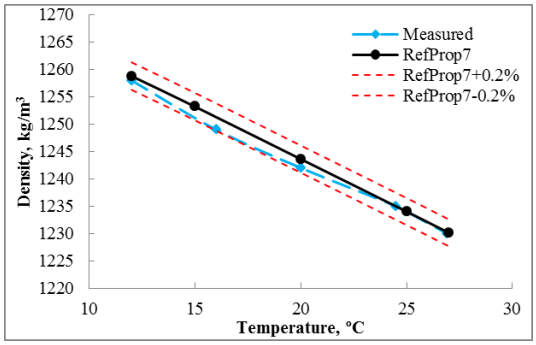

Fig. 1. Comparison of measured density of pure R141b refrigerant with standard data base.

3. Result and Discussion

3.1. Thermal conductivity of nanorefrigerant

Figure 2. (a) shows the thermal conductivity of Al_2O_3/R141b nanorefrigerant at 20ºC temperature for 0.1 to 0.4 volume concentrations of nanoparticles. The experimental result of present study was compared to results obtained from other

models for validation. The figure shows that the thermal conductivity of Al_2O_3/R141b nanorefrigerant was increasing linearly with nanoparticle volume concentration enhancement. The experimental value for this study found to be higher than Maxwell [10] and Yu and Choi [12] models. Moreover, the result of the present study shows lower than Leong et al. [14], Koo and Kleinstreuer [13] and Hamilton and Crosser [11] models. The mean deviation of this experimental value was 0.1 % and 1.38 % with Maxwell [10] and Leong et al. [14] models, respectively.

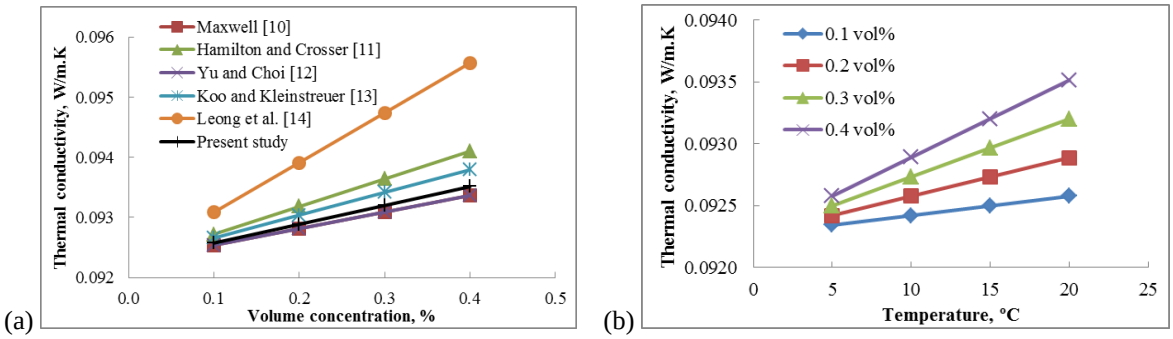

Fig. 2. (a) Thermal conductivity as a function of particle volume fraction; (b) Thermal conductivity as a function of temperature for different volume fraction of nanorefrigerant.

Most of these models were developed based on water as a host fluid. Peng et al. [15] have used Hamilton and Crosser model [11] to predict the thermal conductivity of CuO/R113 nanorefrigerants. Jiang et al. [22] measured the thermal conductivity of CNT/R113 nanorefrigerants. The authors found that, the mean deviation of their experimental value were 15.1 % and 26.9 % with Yu and Choi [12] and Hamilton and Crosser model [11], respectively. Therefore, the thermal conductivity of Al_2O_3/R141b nanorefrigerant in this study was more accurate. However, it can be concluded that the thermal conductivity of nanorefrigerant increases accordingly with the increase of particle volume fraction.

The effect of temperature on the thermal conductivity of nanorefrigerant was investigated by changing the temperatures from 5 to 20ºC. Figure 2. (b) shows the thermal conductivity enhancement of nanorefrigerant at a temperature of 5 to 20ºC for 0.1 to 0.4 volume concentration of nanoparticles. For temperature of 5ºC and particle concentration of 0.1 volume %, the lowest thermal conductivity observed 1.003 times greater than base fluid. The highest thermal conductivity observed 1.013 times greater than base fluid for 20ºC and 0.4 volume concentrations of nanoparticles. The figure shows that the thermal conductivity of nanorefrigerant is proportional to temperature. High nanorefrigerant temperature intensifies the Brownian motion of nanoparticles. With intensified Brownian motion, the contribution of micro convection in heat transport also can be increased. It is evidently shown that the thermal conductivity of nanorefrigerant can be enhanced by increasing the temperature.

3.2. Viscosity of nanorefrigerant

Figure 3. (a) shows the viscosity of Al_2O_3/R141b nanorefrigerant at 20ºC temperature for 0.1 to 0.4 volume concentrations of nanoparticles. It shows viscosity increases linearly with the increase of volume fractions. The experimental result of present study was compared to results obtained from other models for validation. The figure shows that the viscosity of Al_2O_3/R141b nanorefrigerant was increasing linearly with nanoparticle volume concentration enhancement. The experimental value for this study found to be similar with other models. Basically, Einstein model [18] is the pioneering works for predicting suspension viscosity. The other models such as: Brinkman [16], Krieger and Dougherty (K-D) [19], and Batchelor [20] models were developed based on the Einstein model. Moreover, Batchelor model prediction was same for particle concentration less than 2 volume %.

Figure 3. (b) shows the effect of temperature over viscosity of nanorefrigerant. Normally, viscosity of the most of the heat transfer fluid decreases with the increase of temperature. Moreover, viscosity of suspensions decreases with the increase of temperature. The same trend for decrease of viscosity with the increase of temperature was found in this experiment. Some other literatures [23, 24] show the same decreasing trend with the increase of temperature. High nanorefrigerant temperature intensifies the Brownian motion of nanoparticles and reduces the viscosity of nanorefrigerant.

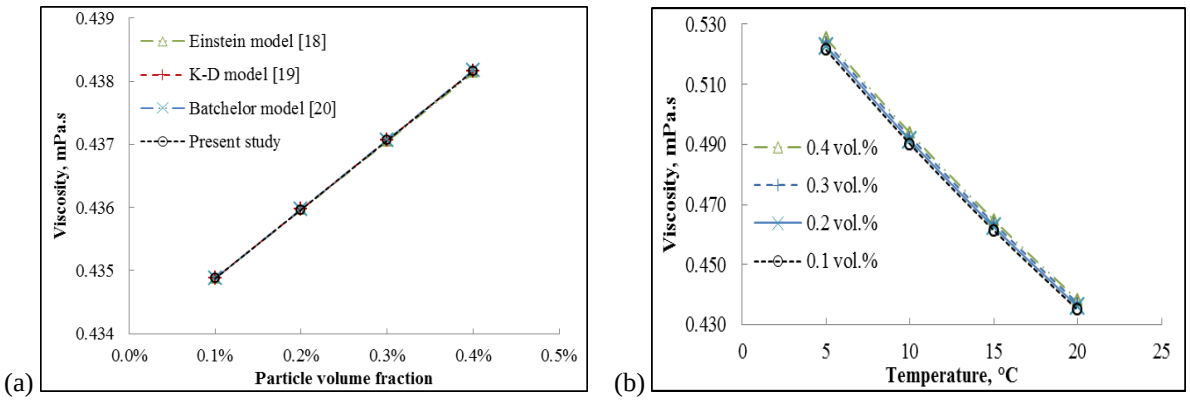

Fig. 3. (a) Viscosity as a function of particle volume fraction; (b) Viscosity as a function of temperature for different volume fraction of nanorefrigerant.

3.3. Density of nanorefrigerant

Figure 4. (a) shows the measured density of Al_2O_3/R141b nanorefrigerant for 0 to 0.4 volume % of Al_2O_3/R141b nanorefrigerant at 20ºC temperature. From the figure, it is clear that, density increases with the increase of volume concentrations. The increment trend was almost linear. Pastoriza-Gallego et al. [25] found the same trend as density increases with the increase of particle concentration for CuO/water nanofluid. Some other experimental result with other base fluid showed the same trend. Wasp et al. [26] and Pak and Cho [27] models were used to compare the experimental data of this study. Figure shows that the experimental value was almost midpoint after 0.1 % volume concentration with the data obtained from these two models. Where, the values of Pak and Cho model was higher than the experimental value and the value of Wasp model was lower than the experimental value. The Pak and Cho model was derived for water based nanofluids and the Wasp model was proposed for metal-lubricant mixture.

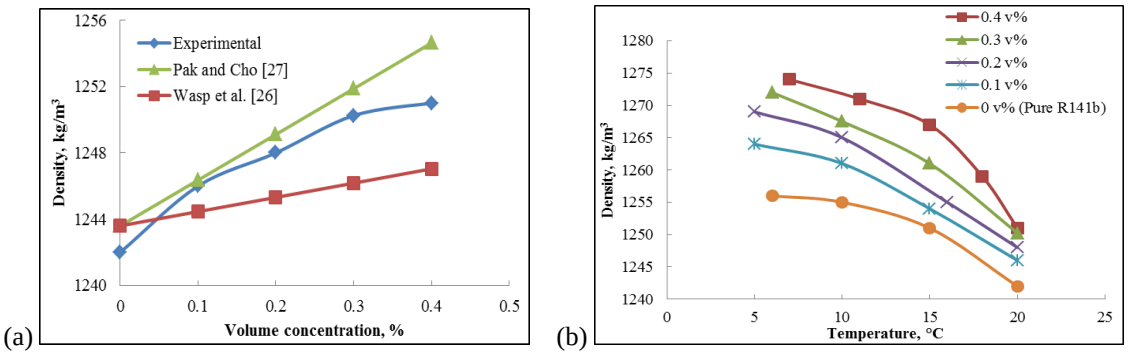

Fig. 4. (a) Density as a function of particle volume fraction; (b) Density as a function of temperature for different volume fraction of nanorefrigerant.

Figure 4. (b) shows the density of Al_2O_3/R141b nanorefrigerant at 5 to 20ºC temperature with 0 to 0.4 volume concentrations of nanoparticles. Figure shows that, density of nanorefrigerant decreases with the increase of temperature. Kedzierski [28] found the same trend as density of suspensions decreases with the increase of temperature for CuO/lubricant nanofluid. It was observed that the decrease trend was slower up to 15ºC and after 15ºC density decreased rapidly.

Conclusion

In this study, attempt was made to investigate the fundamental properties of Al_2O_3/R141b nanorefrigerant. Throughout this study it was found that thermal conductivity of the nanorefrigerant increased with the increase of nanoparticle volume fraction and temperature. It increased sharply due to the intensification of nanoparticle concentration compared to temperature increment.

Results indicate that viscosity increased with the increase of the particle volume fractions. However, it decreased with the increase of temperature. Like the viscosity, density of nanorefrigerant also increases with the enhancement of volume fraction and decreases with the increase of temperature.

From the above results it could be conclude that, an optimal particle volume fraction need to be calculated considering thermal conductivity, viscosity, and density of nanorefrigerant to get efficient energy performances (as thermal conductivity increases the heat transfer coefficients however viscosity and density increases the pressure drop and pumping power). More experimental studies are needed before implementing the nanoparticles in refrigeration systems.

Acknowledgements

The authors acknowledge the financial support from High Impact Research Grant (HIRG) fund under UM-MoHE (Project no. UM.C/HIR/MoHE/ENG/40).

References

[1] Choi, S., 1995. Enhancing thermal conductivity of fluids with nanoparticles, In: Siginer DA, Wang HP (eds). Developments applications of non-newtonian flows, FED-vol 231/MD-vol 66. ASME, New York, P. 99.
[2] Chandrasekar, M., Suresh, S., Chandra Bose, A., 2010. Experimental investigations and theoretical determination of thermal conductivity and viscosity of Al_2O_3/water nanofluid, Experimental Thermal and Fluid Sciences 34, P. 210.
[3] Wang, K., Ding, G., Jiang, W., 2005. "Development of nanorefrigerant and its rudiment property,"- 8th International Symposium on Fluid Control, Measurement and Visualization, Chengdu, China: China Aerodynamics Research Society.
[4] Mahbubul, I.M., Fadhilah, S.A., Saidur, R., Leong, K.Y., Amalina, M.A., 2012. Thermophysical properties and heat transfer performance of Al_2O_3/R-134a nanorefrigerants, International Journal of Heat and Mass Transfer [HMT9361; DOI: 10.1016/j.ijheatmasstransfer.2012.10.007].
[5] Daungthongsuk, W., Wongwisesm S., 2007. A critical review of convective heat transfer of nanofluids, Renewable and Sustainable Energy Reviews 11, p. 797.
[6] Mahbubul, I.M., Saidur, R., Amalina, M.A., 2012. Investigation of viscosity of R123-TiO_2 nanorefrigerant, International Journal of Mechanical and Materials Engineering 7, p. 146.
[7] Saidur, R., Leong, K.Y., Mohammad, H.A., 2011. A review on applications and challenges of nanofluids, Renewable and Sustainable Energy Reviews 15, p. 1646.
[8] Mahbubul, I.M., Saidur, R., Amalina, M.A., 2012. Latest developments on the viscosity of nanofluids, International Journal of Heat and Mass Transfer 55, p. 877.
[9] Sitprasert, C., Dechaumphai, P., Juntasaro, V., 2009. A thermal conductivity model for nanofluids including effect of the temperature-dependent interfacial layer, Journal of Nanoparticle Research 11, p. 1465.
[10] Maxwell, J., A Treatise on Electricity and Magnetisms, 3rd ed. Vol 1, Chap 9, Art 310-314. 1891, Clarendon Press, Oxford p. 435.
[11] Hamilton, R., Crosser, O., 1962. Thermal conductivity of heterogeneous two-component systems, Industrial & Engineering chemistry fundamentals 1, p. 187.
[12] Yu, W., Choi, S., 2003. The role of interfacial layers in the enhanced thermal conductivity of nanofluids: a renovated Maxwell model, Journal of Nanoparticle Research 5, p. 167.
[13] Koo, J., Kleinstreuer, C., 2005. A new thermal conductivity model for nanofluids, Journal of Nanoparticle Research 6, p. 577.
[14] Leong, K., Yang, C., Murshed, S., 2006. A model for the thermal conductivity of nanofluids–the effect of interfacial layer, Journal of Nanoparticle Research 8, p. 245.
[15] Peng, H., Ding, G., Jiang, W., Hu, H., Gao, Y., 2009. Heat transfer characteristics of refrigerant-based nanofluid flow boiling inside a horizontal smooth tube, International Journal of Refrigeration 32, p. 1259.
[16] Brinkman, H., 1952. The viscosity of concentrated suspensions and solutions, The Journal of Chemical Physics 20, p. 571.
[17] Abedian, B., Kachanov, M., 2010. On the effective viscosity of suspensions, International Journal of Engineering Science 48, p. 962.
[18] Einstein, A., 1906. Eine neue bestimmung der moleküldimensionen, Annalen der Physik 324, p. 289.
[19] Krieger, I.M., 1959. A mechanism for non Newtonian flow in suspensions of rigid spheres, Trans Soc Rheol 3: p. 137.
[20] Batchelor, G., 1977. The effect of Brownian motion on the bulk stress in a suspension of spherical particles, Journal of Fluid Mechanics 83, p. 97.
[21] Lemmon, E.W., McLinden, M.O., Huber, M.L., 2002. NIST Reference Fluid Thermodynamic and Transport Properties—Refprop 7.0, NIST Std, in Database: Boulder.
[22] Jiang, W., Ding, G., Peng, H., 2009. Measurement and model on thermal conductivities of carbon nanotube nanorefrigerants. International Journal of Thermal Sciences 48, p. 1108.
[23] Kulkarni, D.P., Das, D.K., Chukwu, G.A., 2006. Temperature dependent rheological property of copper oxide nanoparticles suspension (nanofluid), Journal of Nanoscience and Nanotechnoly, p. 6, 1150.
[24] Namburu, P., Kulkarni, D., Misra, D., Das, D., 2007. Viscosity of copper oxide nanoparticles dispersed in ethylene glycol and water mixture, Experimental Thermal and Fluid Sciences 32, p. 397.
[25] Pastoriza-Gallego, M.J., Casanova, C., Legido, J.L., Piñeiro, M.M., 2011. CuO in water nanofluid: Influence of particle size and polydispersity on volumetric behaviour and viscosity, Fluid Phase Equilibria 300, p. 188.
[26] Wasp, E., Kenny, J., Gandhi, R., 1977. Solid-liquid flow slurry pipeline transportation, Series on Bulk Materials Handling 1, p. 56.
[27] Pak, B.C., Cho, Y.I., 1998. Hydrodynamic and heat transfer study of dispersed fluids with submicron metallic oxide particles, Experimental Heat Transfer 11, p. 151.
[28] Kedzierski, M.A., 2009. "Viscosity and density of CuO nanolubricant", in Third conference on thermophysical properties and transfer processes of refrigerants, Boulder, CO.

Available online at www.sciencedirect.com

SciVerse ScienceDirect

Procedia Engineering 00 (2012) 000–000

Procedia Engineering

www.elsevier.com/locate/procedia

5th BSME International Conference on Thermal Engineering

Effects of Magnetic Field on Radiative Flow of a Nanofluid past a Stretching Sheet

Md. Shakhaoath Khan[a] , Md. Mahmud Alam[b,*] and M. Ferdows[c]

[a,b] *Mathematics Discipline; Science, Engineering and Technology School, Khulna University, Khulna-9208, Bangladesh*

[c] *Department of Mathematics, University of Dhaka, Dhaka-1000, Bangladesh*

Abstract

Unsteady laminar boundary-layer flows of a nanofluid past a stretching sheet with thermal radiation in the presence of magnetic field have been studied numerically. The non-similar momentum, energy and concentration equations have been obtained by using non-dimensional variables. The non-similar equations are presented here which depends on the useful parameters of the model. The obtained equations have been solved by explicit finite difference method with stability and convergence analysis. The velocity, temperature and nanoparticles volume fraction profiles as well as the average Shear stress, Nusselt number and Sherwood number at the sheet are discussed for the different values of important parameters with different time steps.

Keywords: Nanofluid; Magnetic field; Thermal Radiation; Stretching sheet

Nomenclature

v	velocity components	υ	kinematic viscosity
ρ	density of fluid	t	time
τ	dimensionless time	$\bar{U}$	dimensionless velocity
$\bar{T}$	dimensionless temperature	$\bar{C}$	dimensionless volume fraction
q_r	radiative heat flux in the y-direction	M	Magnetic Parameter
R	Radiation parameter	P_r	Prandtl number
E_c	Eckert number	L_e	Lewis Number
N_b	Brownian motion parameter	N_t	Thermophoresis parameter

1. Introduction

The study of Radiative heat transfer in nanofluids is gaining a lot of attention. Moreover the investigation on Magnetohydrodynamics (MHD) boundary layer flow over a stretching sheet has attracted considerable attention during the last few decades due to its numerous applications in industrial manufacturing processes such as the aerodynamic extrusion of plastic sheets, liquid film, hot rolling, wire drawing, glass-fiber and paper production, drawing of plastic films, metal and polymer extrusion and metal spinning. Sakiadis [1] was the first one to analyze the boundary layer flow on

* Corresponding author. Tel.: +88-041-2831544; fax: +88-041-731244.
E-mail address: alam_mahmud2000@yahoo.com

continuous surfaces. Crane [2] obtained an exact solution the boundary layer flow of Newtonian fluid caused by the stretching of an elastic sheet moving in its own plane linearly. El-Kabeir [3] studied the interaction of forced convection and thermal radiation during the flow of a surface moving continuously in a flowing stream of micropolar fluid with variable viscosity. The nanofluids have many applications in the industries since materials of nanometer size have unique physical and chemical properties. Nanofluids are solid-liquid composite materials consisting of solid nanoparticles (or nanofibers with sizes typically of 1-100 nm) suspended in liquid. Nanofluids have attracted great interest recently because of reports of greatly enhanced thermal properties. A small amount (< 1% volume fraction) of Cupper (Cu) nanoparticles or carbon nanotubes dispersed in ethylene glycol or oil is reported to increase the inherently poor thermal conductivity of the liquid by 40% and 150% respectively (Choi et al., [4]). The interdisciplinary nature of nanofluid research presents a great opportunity for exploration and discovery at the frontiers of nanotechnology. Khan and Pop [5, 6] analyzed the development of the steady boundary layer flow, heat transfer and nanoparticle fraction over a stretching surface in a Nanofluid. Kuznetsov and Nield [7] have studied the classical problem of free convection boundary layer flow of a viscous and incompressible fluid (Newtonian fluid) past a vertical flat plate to the case of nanofluids. Syakila and Pop [8] studied the steady mixed convection boundary layer flow past a vertical flat plate embedded in a porous medium filled with nanofluids. Bachok et al. [9] have investigated the steady boundary-layer flow of a nanofluid past a moving semi-infinite flat plate in a uniform free Stream. Tiwari and Das [10] have investigated the natural convection in partially heated rectangular enclosures filled with nanofluids. Duangthongsuk and Wongwises [11] analyzed the effect of thermophysical properties models on the predicting of the convective heat transfer coefficient for low concentration nanofluid. Gorla et al. [12] have studied mixed convective boundary layer flow over a vertical wedge embedded in a porous medium saturated with a nanofluid.

The aim of the present study is to analyze the effects of magnetic field and thermal radiation on unsteady boundary layer nanofluid flow over a stretching surface. Explicit finite difference method (Carnahan et al. [13]) has been used to solve the obtained non- similar equations.

2. Mathematical Model of the flow

Considered the Cartesian coordinates x, measured along the stretching surface and y is the coordinate measured normal to the stretching surface. The physical configuration and coordinate system are shown in Fig. 1 (from Khan and Pop [5], Fig 1). The flow takes place at $y \geq 0$. An unsteady uniform stress leading to equal and opposite forces is applied along the x-axis, so that the sheet is stretched keeping the origin fixed. Initially it is assumed that fluid and the plate are at rest after that the plate is moved with a constant velocity U_0 in its own plane. Instantaneously at time $t > 0$, temperature of the plate and species concentration are raised to $T_w\left(>T_\infty\right)$ and $C_w\left(>C_\infty\right)$ respectively, which are thereafter maintained constant, where T_w, C_w are temperature and species concentration at the wall and T_∞, C_∞ are temperature and species concentration far away from the plate respectively. A uniform magnetic field B_0 is imposed to the plate. The magnetic induction vector B_0 can be taken as $B=\left(0,B_0,0\right)$.And q_r is the radiative heat flux in the y-direction. Under the usual boundary layer approximation, the MHD unsteady nanofluid flow and heat and mass transfer with the radiation effect are governed by the following equations;

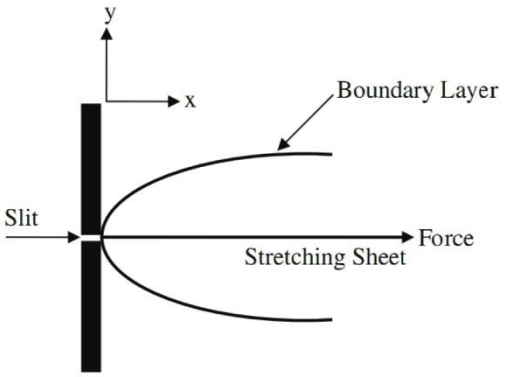

Fig. 1. Physical Configuration and coordinates system

$$\frac{\partial v}{\partial y}=0 \tag{1}$$

$$\frac{\partial u}{\partial t}+v\frac{\partial u}{\partial y}=\upsilon\frac{\partial^2 u}{\partial y^2}-\frac{\sigma {B_0}^2}{\rho}u \tag{2}$$

$$\frac{\partial T}{\partial t}+v\frac{\partial T}{\partial y}=\alpha\frac{\partial^2 T}{\partial y^2}-\frac{\alpha}{k}\frac{\partial q_r}{\partial y}+\frac{\upsilon}{c_p}\left(\frac{\partial u}{\partial y}\right)^2+\tau\left\{D_B\left(\frac{\partial T}{\partial y}\cdot\frac{\partial C}{\partial y}\right)+\frac{D_T}{T_\infty}\left(\frac{\partial T}{\partial y}\right)^2\right\} \tag{3}$$

$$\frac{\partial C}{\partial t}+v\frac{\partial C}{\partial y}=D_B\frac{\partial^2 C}{\partial y^2}+\frac{D_T}{T_\infty}\frac{\partial^2 T}{\partial y^2} \tag{4}$$

the initial and boundary conditions are;

$$\begin{aligned} &t \le 0, u_w = v_\circ = ax,, T = T_\infty, C = C_\infty && \text{everywhere} \\ &t > 0, u = v_\circ = ax, T = T_\infty, C = C_\infty, && \text{at } x = 0 \\ &\quad u = 0, T \to T_\infty, C \to C_\infty, && \text{as } y \to \infty \end{aligned} \tag{5}$$

where α is the thermal diffusivity, k is the thermal conductivity, D_B is the Brownian diffusion coefficient, D_T is the thermophoresis diffusion coefficient, where, x is the coordinate measured along stretching surface, u_w is the stretching velocity, U is the uniform velocity and $v = -v_\circ$ is the constant suction velocity.

The Rosseland approximation (Brewster, [14]) is expressed for radiative heat flux and leads to the form as,

$$q_r = -\frac{4\sigma}{3\kappa^*}\frac{\partial T^4}{\partial y} \tag{6}$$

where σ is the Stefan-Boltzmann constant and κ^* is the mean absorption coefficient. The temperature difference with in the flow is sufficiently small such that T^4 may be expressed as a linear function of the temperature, then the Taylor's series for T^4 about T_∞ after neglecting higher order terms,

$$T^4 = 4T_\infty{}^3 - 3T_\infty{}^4 \tag{7}$$

Introducing the following non dimensional variables;

$$Y = \frac{yv_0}{\upsilon},\ \bar{U} = \frac{u}{v_0},\ \tau = \frac{tv_0^2}{\upsilon},\ \bar{T} = \frac{T - T_\infty}{T_w - T_\infty},\ \bar{C} = \frac{C - C_\infty}{C_w - C_\infty}.$$

Therefore the equations (1) to (5) become;

$$\frac{\partial V}{\partial Y} = 0 \tag{8}$$

$$\frac{\partial \bar{U}}{\partial \tau} - \frac{\partial \bar{U}}{\partial Y} = \frac{\partial^2 \bar{U}}{\partial Y^2} - M\bar{U} \tag{9}$$

$$\frac{\partial \bar{T}}{\partial \tau} - \frac{\partial \bar{T}}{\partial Y} = \left(\frac{1+R}{P_r}\right)\frac{\partial^2 \bar{T}}{\partial Y^2} + E_c\left(\frac{\partial \bar{U}}{\partial Y}\right)^2 + N_b\left(\frac{\partial \bar{T}}{\partial Y}\cdot\frac{\partial \bar{C}}{\partial Y}\right) + N_t\left(\frac{\partial \bar{T}}{\partial Y}\right)^2 \tag{10}$$

$$\frac{\partial \bar{C}}{\partial \tau} - \frac{\partial \bar{C}}{\partial Y} = \frac{1}{L_e}\left[\frac{\partial^2 \bar{C}}{\partial Y^2} + \left(\frac{N_t}{N_b}\right)\frac{\partial^2 \bar{T}}{\partial Y^2}\right] \tag{11}$$

the non-dimensional boundary conditions are;

$$\tau \le 0,\ U = 0,\ \bar{T} = 0,\ \bar{C} = 0 \qquad \text{everywhere} \tag{12}$$

$$\tau > 0, U = 1, \bar{T} = 1,\ \bar{C} = 1 \qquad \text{at } Y = 0 \tag{13}$$

$$U = 0, \bar{T} = 0,\ \bar{C} = 0 \qquad \text{as } Y \to \infty$$

where, Magnetic parameter $M = \frac{\sigma B_0{}^2 \nu}{\rho v_0^2}$, Radiation parameter $R = \frac{16\sigma T_\infty{}^3}{3k\kappa^*}$, Prandtl number $P_r = \frac{\upsilon}{\alpha}$, Eckert number $E_c = \frac{v_0{}^2}{c_p(T_w - T_\infty)}$, Lewis number $L_e = \frac{\upsilon}{D_B}$, Brownian parameter $N_b = \frac{\tau D_B}{\upsilon}(C_w - C_\infty)$ and Thermophoresis parameter $N_t = \frac{D_T}{T_\infty}\frac{\tau}{\nu}(T_w - T_\infty)$.

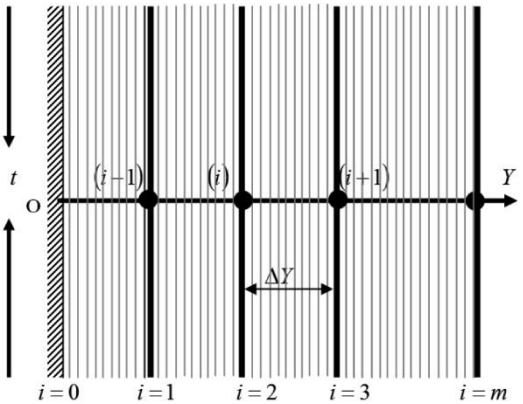

Fig. 2. Finite difference space grid

3. Numerical Technique

To solve the governing second order coupled dimensionless partial differential equations (9)-(11) with the associated initial and boundary conditions the explicit finite difference method has been used. The present problem is required a set of finite difference equation. In this case the region within the boundary layer is divided by some perpendicular lines of $Y-$axis, where $Y-$axis is normal to the medium as shown in Fig. 2. It is assumed that the maximum length of boundary layer is $Y_{\max}(=20)$ as corresponds to $Y \to \infty$. i.e. Y varies from 0 to 20 and the number of grid spacing in Y directions is

$m(=100)$, hence the constant mesh size along Y axis becomes $\Delta Y = 0.20$ $(0 \le Y \le 20)$ with a smaller time step $\Delta t = 0.005$. Let $\overline{U}^n$, $\overline{T}^n$ and $\overline{C}^n$ denote the values of $\overline{U}$, $\overline{T}$ and $\overline{C}$ at the end of a time-step respectively. Using the explicit finite difference approximation, the following appropriate set of finite difference equations are obtained as;

$$\frac{\overline{U}_i^{n+1}-\overline{U}_i^n}{\Delta\tau}-\frac{\overline{U}_{i+1}^n-\overline{U}_i^n}{\Delta\overline{Y}}=\frac{\overline{U}_{i+1}^n-2\overline{U}_i^n+\overline{U}_{i-1}^n}{\left(\Delta\overline{Y}\right)^2}-M\overline{U}_i^n \tag{14}$$

$$\frac{\overline{T}_i^{n+1}-\overline{T}_i^n}{\Delta\tau}-\frac{\overline{T}_{i+1}^n-\overline{T}_i^n}{\Delta\overline{Y}}=\left(\frac{1+R}{P_r}\right)\frac{\overline{T}_{i+1}^n-2\overline{T}_i^n+\overline{T}_{i-1}^n}{\left(\Delta\overline{Y}\right)^2}+E_c\left(\frac{\overline{U}_{i+1}^n-\overline{U}_i^n}{\Delta\overline{Y}}\right)^2+N_b\left(\frac{\overline{T}_{i+1}^n-\overline{T}_i^n}{\Delta\overline{Y}}\cdot\frac{\overline{C}_{i+1}^n-\overline{C}_i^n}{\Delta\overline{Y}}\right)+N_t\left(\frac{\overline{T}_{i+1}^n-\overline{T}_i^n}{\Delta\overline{Y}}\right)^2 \tag{15}$$

$$\frac{\overline{C}_i^{n+1}-\overline{C}_i^n}{\Delta\tau}-\frac{\overline{C}_{i+1}^n-\overline{C}_i^n}{\Delta\overline{Y}}=\frac{1}{L_e}\left[\frac{\overline{C}_{i+1}^n-2\overline{C}_i^n+\overline{C}_{i-1}^n}{\left(\Delta\overline{Y}\right)^2}+\left(\frac{N_t}{N_b}\right)\frac{\overline{T}_{i+1}^n-2\overline{T}_i^n+\overline{T}_{i-1}^n}{\left(\Delta\overline{Y}\right)^2}\right] \tag{16}$$

and the initial and boundary conditions with the finite difference scheme are

$$\overline{U}_i^0=0,\quad \overline{T}_i^0=0,\quad \overline{C}_i^0=0 \tag{17}$$

$$\overline{U}_0^n=1,\quad \overline{T}_0^n=1,\quad \overline{C}_0^n=1$$
$$\overline{U}_L^n=0,\quad \overline{T}_L^n=0,\quad \overline{C}_L^n=0 \quad \text{where, } L\to\infty \tag{18}$$

Here the subscripts i designate the grid points with Y coordinates and the superscript n represents a value of time, $\tau = n\Delta\tau$ where $n = 0,1,2,3,4,.....$. From the initial condition (17), the values of $\overline{U}^n$, $\overline{T}^n$ and $\overline{C}^n$ are known at $\tau = 0$. At the end of any time-step $\Delta\tau$, the new temperature $\overline{T}^{n+1}$, the new concentration $\overline{C}^{n+1}$, the new velocity $\overline{U}^{n+1}$, at all interior nodal points may be obtained by successive applications of equations (14), (15) and (16) respectively. This process is repeated in time and provided the time-step is sufficiently small $\overline{U}^n$, $\overline{T}^n$ and $\overline{C}^n$ should eventually converge to values which approximate the solution of equations (14) to (16). Also the numerical values of the average Shear Stress (τ_A), average Nusselt number (N_{uA}) and average Sherwood number (S_{hA}) are evaluated as follows;

$$\tau_A=\int\left(\frac{\partial u}{\partial y}\right)_{y=0}dx;\quad N_{uA}=(1+R)\int\left(-\frac{\partial T}{\partial y}\right)_{y=0}dx;\quad S_{hA}=\int\left(-\frac{\partial C}{\partial y}\right)_{y=0}dx \tag{19}$$

The stability conditions of the method are,

$$\frac{2(1+R)}{P_r}\frac{\Delta\tau}{(\Delta Y)^2}+2N_b\overline{C}\frac{\Delta\tau}{(\Delta Y)^2}+2N_t\overline{T}\frac{\Delta\tau}{(\Delta Y)^2}\le 1 \text{ and } \frac{\Delta\tau}{\Delta Y}+\frac{2}{L_e}\frac{\Delta\tau}{(\Delta Y)^2}\le 1. \tag{20}$$

The convergence criteria of the method are $P_r \ge 0.35$ and $L_e \ge 0.25$.

4. Results and Discussion

To observe the physical significance of the model, the numerical values of velocity $(\overline{U})$, temperature $(\overline{T})$ and nanoparticles volume fraction $(\overline{C})$ have been computed within the boundary layer for different values of Magnetic parameter M, Radiation parameter R, Prandtl number P_r, Eckert number E_c, Lewis number L_e, Brownian motion parameter N_b and Thermophoresis parameter N_t. To obtain the steady state solution, the computation have been carried out up to non-dimensional time, $\tau = 80$. The velocity, temperature and nanoparticles volume fraction profiles doesn't show any change after non-dimensional time, $\tau = 50$. Therefore the solution for $\tau \ge 50$ is steady-state solution. The graphical representation of the problem has been showed in Figs. 3-10.

Fig. 3 displays the effect of *M* on the velocity profiles for the different time step. It can be seen that, the velocity of the fluid decreases as *M* increase. It occurs when the momentum boundary layer decreases. Figs. 4 and 5 show the temperature profiles for the different time step and different values of *R* and E_c respectively. It can be observed that the increasing value of *R* and E_c caused the rising effects on temperature profiles respectively. Since the nanofluid temperature is merely due to stretching of the sheet, it satisfies the boundary condition at $\eta = \infty$. Fig. 6 displays the effect of L_e on the

nanoparticle volume fraction profiles. It can be seen that, nanoparticle volume fraction profiles decreases as L_e increase.

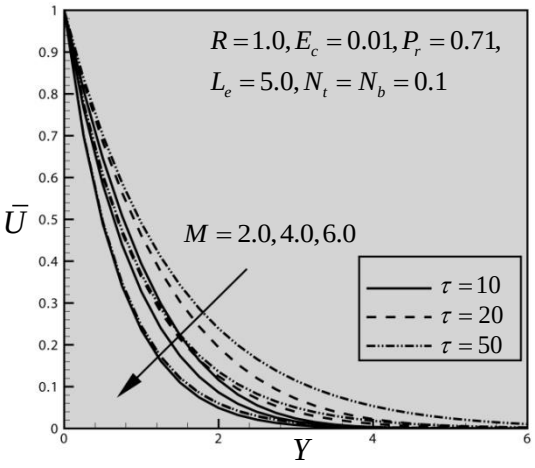

Fig. 3. Effect of M on velocity profiles

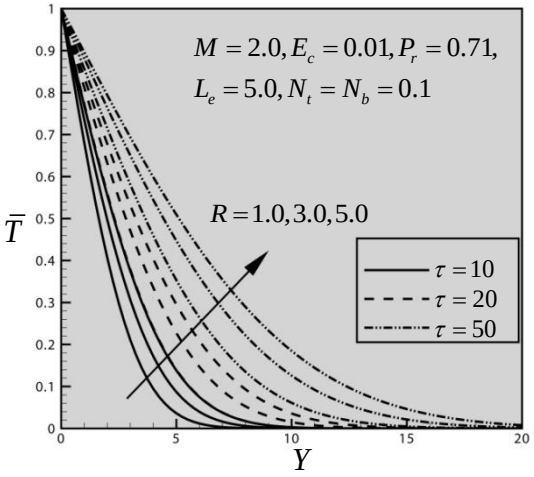

Fig. 4. Effect of R on temperature profiles

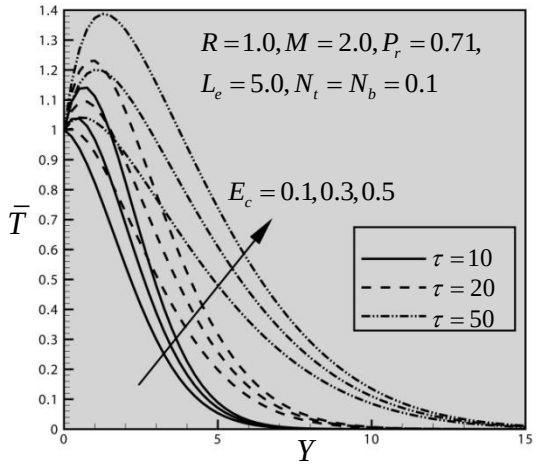

Fig. 5. Effect of E_c on temperature profiles

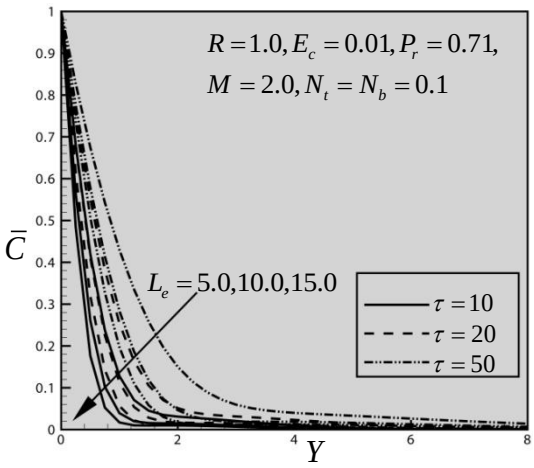

Fig. 6. Effect of L_e on concentration profiles

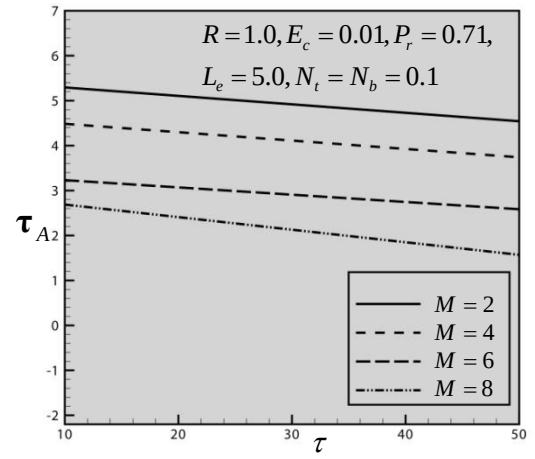

Fig. 7. Average shear stress for different M

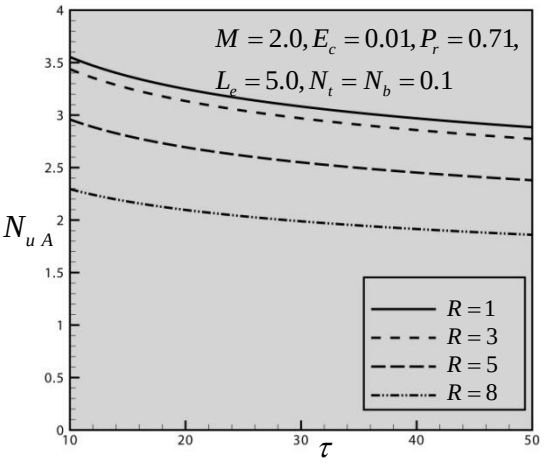

Fig. 8. Average Nusselt number for different R

The behaviour of the quantities of chief physical interest as the average shear stress τ_A, average Nusselt number $N_{u\,A}$ and average Sherwood number $S_{h\,A}$ verses τ are illustrated in Figs. 7-10 for different values of magnetic parameter, Radiation parameter, Eckert number and Brownian motion parameter respectively. Fig. 7 depicts average shear stress τ_A decreases with the increase of M. In Fig. 8, average Nusselt number $N_{u\,A}$ decreases gradually for increasing the different values

of R . As E_c increases average Nusselt number $N_{u\,A}$ increases in Fig 9. Also in Fig 10, average Sherwood number $S_{h\,A}$ increases gradually for increasing the different values of N_b .

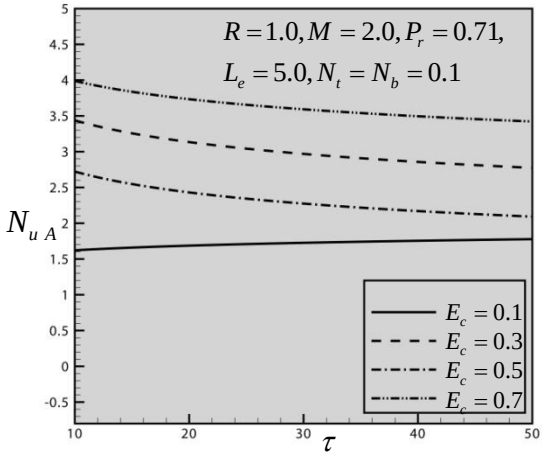

Fig. 9. Average Nusselt number for different E_c

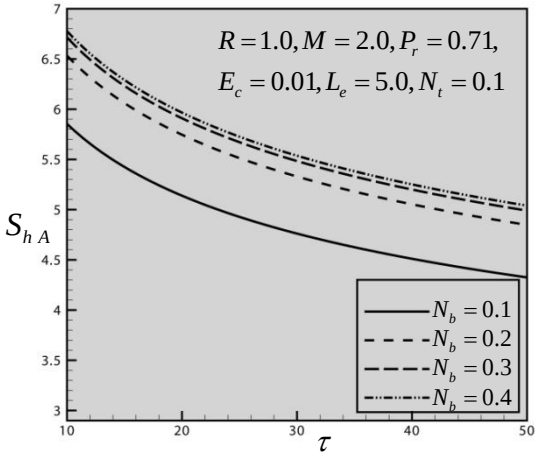

Fig. 10. Average Sherwood number for different N_b

5. Conclusions

This paper investigated the effect of magnetic field and thermal radiation on boundary layer heat and mass transfer flow over an unsteady stretching surface. Numerical calculations are carried out for various values of the dimensionless parameters. The effects of various physical parameters on the heat and mass transfer characteristics were examined. The momentum boundary layer thickness and average shear stress reduce as Magnetic parameter is increased. The increase of thermal radiation parameter is caused to the rise of thermal boundary layer thickness. The thermal boundary layer thickness and the rate of heat transfer increase as increasing the Eckert number.

Acknowledgements

The authors wish to express their very sincerely thanks to the reviewers and the 5th BSME ICTE committee for their valuable comments and suggestions.

References

[1] Sakiadis, BC., 1961. Boundary-layer behavior on a continuous solid surface: II-The boundary layer on a continuous flat surface, AIChE Journal 7, p. 221-225.
[2] Crane, LJ., 1970. Flow Past a Stretching Plate, ZAMP 21, p. 645-647.
[3] EL-Kabeir SMM., 2004. Radiative effects on forced convection flows in micropolar fluids with variable viscosity, Can. J. Phys 82, p. 151-165.
[4] Choi SUS, Zhang ZG, Yu W, Lockwood FE, Grulke EA., 2001. Anomalous thermal conductivity enhancement on nanotube suspensions, Appl Phys Lett. 79, p. 2252-2254.
[5] Khan WA, Pop I., 2010. Boundary layer flow of nanofluid past a stretching sheet, Int. J. Of Heat and Mass Transfer 53, p. 2477-2483.
[6] Khan WA, Pop I., 2011. Free Convection Boundary Layer Flow Past a Horizontal Flat Plate Embedded in a Porous Medium Filled with a Nanofluid, J. Heat Trans. p. 133: 9.
[7] Kuznetsov AV, Nield DA., 2010. Natural convective boundary-layer flow of a nanofluid past a vertical plate, International Journal of Thermal Sciences 49, p. 243-247.
[8] Syakila Ahmed, Pop I., 2010. Mixed convection boundary layer flow from a vertical flat plate embedded in a porous medium filled with nanofluids, Int. Commun. in Heat and Mass Transfer 37, p. 987-991.
[9] Bachok N, Ishak A, Pop I., 2007. Boundary layer flow of nanofluid over moving surface in a flowing fluid, Int. J. of Thermal Sciences 49, p. 1663-1668.
[10] Tiwari RK, Das MK., 2007. Heat transfer augmentation in a two-sided lid-driven differentially heated square cavity utilizing nanofluids, International Journal of Heat and Mass Transfer 50, p. 2002-2018.
[11] Duangthongsuk W, Wongwises S., 2008. Effect of thermophysical properties models on the predicting of the convective heat transfer coefficient for low concentration nanofluid, International Communications in Heat and Mass Transfer 35, p. 1320-1326.
[12] Gorla RSR, Chamkha AJ, Rashad AM., 2011. Mixed convective boundary layer flow over a vertical wedge embedded in a porous medium saturated with a nanofluid: Natural Convection Dominated Regime, Nanoscale Research Letters 6, p. 207.
[13] Carnahan B, Luther HA, Wilkes JO., 1969. Applied Numerical Methods. John Wiley and sons, New York.
[14] Brewster MQ., 1992. Thermal Radiative Transfer and Properties. John Wiley and Sons Inc., New York: USA.

Available online at www.sciencedirect.com

SciVerse ScienceDirect

Procedia Engineering 00 (2012) 000–000

Procedia Engineering

www.elsevier.com/locate/procedia

5th BSME International Conference on Thermal Engineering

Heat transfer and pressure drop characteristics of Al_2O_3-R141b nanorefrigerant in horizontal smooth circular tube

I.M. Mahbubul[a]*, R. Saidur[a,b], M.A. Amalina[a]

[a]*Department of Mechanical Engineering, University of Malaya, 50603 Kuala Lumpur, Malaysia*
[b]*UM Power Energy Dedicated Advanced Centre (UMPEDAC), Level 4, Wisma R&D, University of Malaya, 59990 Kuala Lumpur, Malaysia*

Abstract

Since 1995, research has been going on in different aspects of nanofluids. Most of them are related to thermal conductivity and heat transfer properties of nanofluids based on water or ethylene glycol. Nanorefrigerants are one kind of promising nanofluids that based on refrigerants. Hear transfer and pressure drop characteristics of nanorefrigerants must be determined before putting into application. The objectives of this study are to determine the heat transfer and pressure drop characteristics of Al_2O_3-R141b nanorefrigerants for different volume concentrations. The experimental conditions include: constant mass flux of 100 $kgm^{-2}s^{-1}$, vapor qualities from 0.2 to 0.7, temperature at 25°C and 0.078535 MPa pressure. Based on the analysis it was found that both heat transfer and pressure drop characteristics increased with the enhancement of nanoparticle volume concentrations. Therefore, an optimum concentration of nanoparticles with refrigerants (compromising the heat transfer performance and pressure drop characteristics) can improve the performance of a refrigeration system as to increase the energy efficiency and cooling capacity.

Keywords: Nanofluid; Volume concentration; Vapor quality; Flow boiling heat transfer coefficient.

1. Introduction

Nanofluid is a new dimensional thermo fluid that has emerged after the pioneering work by Choi [1]. Nanofluid is a solid-liquid mixture that consists of a nanoparticles and a base liquid. The nanorefrigerant is one kind of nanofluid and its host fluid is refrigerant [2]. Refrigerants are widely used in refrigeration and air conditioning equipment in industries, offices, and domestic and commercial buildings. Nanorefrigerants are potential to enhance heat transfer rate thus making air conditioning and refrigeration systems more efficient. This consequently will reduce energy consumption in these sectors along with reduction in emissions and global warming potential. However, there are some penalties like pressure drop and pumping power increases for using the nanoparticles in refrigeration system. Therefore, both the heat transfer and pressure drop characteristics must need to be calculated before implementing the nanoparticles in refrigeration system [3]. The investigations of heat transfer coefficients are important to increase the energy efficiency of a refrigeration system especially in heat exchangers which involved phase-change of working fluid. By suspending nanoparticles into the refrigerant, the heat transfer coefficient increased as the mixture change the properties of nanorefrigerants [4]. Carbon Nanotubes (CNTs) that have high thermal conductivity show high heat transfer coefficient enhancement. Park and Jung [5] investigated pool boiling heat transfer coefficients of CNTs/R-123 and CNTs/R-134a nanorefrigerants where heat transfer coefficient enhanced about 36.6 % at low heat flux. The investigation of Al_2O_3 in R-134a/polyolester mixtures on a roughened, horizontal and flat surface enhanced the pool boiling heat transfer coefficient about 400 % at heat flux of 7

* Corresponding author. Tel.: +6 03 7967 7611; fax: +6 03 7967 5317.
E-mail address: mahbub_ipe@yahoo.com

kW/m^2 [6]. Henderson et al. [7] investigated the effect of SiO_2 nanoparticles with volume fraction of 0.02 to 0.08 % on two phase flow boiling heat transfer coefficient of R-134a and R-134a/polyolester. The mixtures of nanoparticles with R-134a refrigerant through direct dispersion decreased 55 % of heat transfer coefficient compared to pure R-134a refrigerant.

Pressure drop investigation is also quite important in order to have an accurate design and optimization of a refrigeration system [8]. The investigation of the two-phase pressure drop can involve direct expansion evaporator, condenser and transfer lines. Peng et al. [9] investigated the frictional pressure drop of R-113 refrigerant with 0 – 0.5 wt % suspension of CuO nanoparticle. Their investigation show that the pressure drop increases with nanoparticle concentration and the maximum enhancement is 20.8 %. A new frictional pressure drop correlation for nanorefrigerants has been developed from the same study that can be applied to investigate the frictional pressure drop of any nanorefrigerant.

To the best of authors knowledge there is no literature available that considered both the heat transfer and pressure drop characteristics of refrigerant based nanofluids. The objective of this paper is to investigate the heat transfer and pressure drop characteristics of Al_2O_3/R141b nanorefrigerant.

2. Methodology

The properties of Al_2O_3 nanoparticles and R141b refrigerant have tabulated in Table 1. Refrigerant properties were taken from REFPROP7 standard data base [10]. Some constant parameters of nanorefrigerant flows inside a horizontal tube have presented in Figure 1. The investigations of nanorefrigerant performance are based on the influence of Al_2O_3 nanoparticles of 1 to 5 volume concentration and the average diameter of nanoparticles was 13 nm throughout the analyses. The nanorefrigerant was assumed to flow at constant velocity of 5 m/s and the vapor quality was from 0.2 to 0.7. No surfactant was considered for dispersion of refrigerant-based nanofluids. Thus, the effect of surfactant was neglected during the analyses. Referring to the mathematical models of nanofluids and nanorefrigerant from various sources, investigation of Al_2O_3/R141b nanorefrigerant characteristics have been conducted by using Microsoft Excel 2010.

Table 1. Properties of Al_2O_3 nanoparticles and R41b refrigerant at 25ºC and 78.535 kPa.

Property	Unit	Al_2O_3	R141b	R141b (liquid)	R141b (vapour)
Chemical formula	-	Al_2O_3	CH3CCL2F	CH3CCL2F	CH3CCL2F
Normal Boiling point	ºC	-	32.06	-	-
Molecular mass	g/mol	101.96	116.95	-	-
Density	kg/m^3	4260	-	1234	3.826
Viscosity	mPa.s	-	-	0.40932	0.0091878
Thermal conductivity	W/m.K	40	-	0.090842	0.0098663
Specific heat	J/kg.K	773	-	1.1538	0.7854
Surface tension	N/m	-	0.018355	-	-

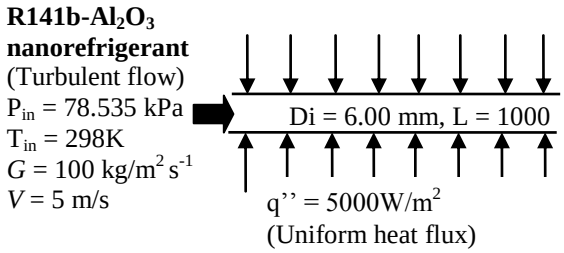

Fig. 1. Test condition-Uniformly heated flow in a horizontal smooth tube.

2.1. Flow boiling heat transfer coefficient calculation

A correlation from Peng et al. [11] was used to calculate the flow boiling heat transfer coefficient,

$$\alpha_{r,n} = F_{HT}.\alpha_r \tag{1}$$

Where, F_{HT} is the nanoparticle impact factor; and α_r is the heat transfer coefficient of pure refrigerant. The nanoparticle impact factor is a function of particle volume fraction, thermophysical properties of nanoparticle and refrigerant, vapor quality as well as mass flux and it can be determined by,

$$F_{HT} = \exp\left\{\phi\left[0.8\frac{k_p}{k_r} - 39.94\frac{(\rho C_p)_p}{(\rho C_p)_{r,L}} - 0.028G - 733.26x(1-x)\right]\right\} \tag{2}$$

Where, ϕ is the particle volume concentration; k_p and k_r are the thermal conductivity of solid particles and pure refrigerant, respectively; ρ is the density and C_p is the specific heat of particle ($_p$) and liquid phase refrigerants ($_{r,L}$). G is the mass flux and x is the vapor quality. In order to find the flow boiling heat transfer coefficient of pure refrigerant, a correlation from Saitoh et al. [12] was used:

$$\alpha_r = Fh_L + Sh_{pool} \tag{3}$$

Heat transfer coefficient is the combination of convective boiling contribution, Fh_L and a nucleate boiling contribution, Sh_{pool}. From equation (3), h_L is the heat transfer coefficient based on the Dittus-Boelter's equation [13] for liquid flow in the tube which can be calculated from:

$$h_L = \frac{4.36k_r}{D_i} \text{ for } \mathrm{Re} < 1000 \tag{4}$$

$$h_L = 0.023\frac{k_r}{D_i}\left(\frac{GD_i}{\mu_r}\right)^{0.8}\left(\frac{(C_p)_{r,L} - \mu_r}{k_r}\right)^{1/3} \text{ for } \mathrm{Re} > 1000 \tag{5}$$

Where, μ_r is the viscosity of pure refrigerant, D_i is the internal diameter of tube. The enhancement factor *F* was calculated by,

$$F = 1 + \frac{\left(\frac{1}{x}\right)^l}{1 + We_G^m} \tag{6}$$

Where, X is Lockhart Martinelli Parameter and We_G^m is the Weber number with *m* and *l* are equal to -0.4 and 1.05, respectively. Value of X , was calculated by:

$$X = \left(\frac{1-x}{x}\right)^{0.9}\left(\frac{\rho_G}{\rho_{r,L}}\right)^{0.5}\left(\frac{\mu_r}{\mu_G}\right)^{0.1} \tag{7}$$

$$We_G = \frac{G^2 D_i}{\sigma\rho_G} \tag{8}$$

Where, σ is the surface tension of refrigerant. The Suppression factor, S was determined by

$$S = \frac{1}{1 + a\left(\mathrm{Re}_{TP} \times 10^{-4}\right)^n} \tag{9}$$

Where, $a = 0.4$ and $n = 1.4$. Re_{TP} is two phase Reynolds number which was calculated by multiplying the Reynolds number and enhancement factor, F as shown below:

$$\mathrm{Re}_{TP} = \mathrm{Re}_L F^{1.25} \tag{10}$$

The pool boiling heat transfer coefficient h_{pool} was determined from the following equation:

$$h_{pool} = 207 \frac{k_r}{d_b} \left(\frac{q'' d_b}{k_r T_r} \right)^{0.745} \left(\frac{\rho_G}{\rho_{r,L}} \right)^{0.581} \mathrm{Pr}_r^{0.533} \tag{11}$$

Where, q'' is the heat flux, T_r is the refrigerant temperature, Pr_r is the Prandlt number of refrigerant and d_b is the bubble departure diameter of nucleate boiling and it can be determined as following:

$$d_b = 0.51 \left[\frac{2\sigma}{g(\rho_{r,L} - \rho_G)} \right]^{0.5} \tag{12}$$

Where, g is the gravitational acceleration with a constant value of 9.81m/s^2.

2.2. *Pressure drop calculation*

The correlation proposed by Peng et al. [9] was used to investigate the pressure drop characteristics of Al_2O_3/R141b nanorefrigerants flow boiling inside a horizontal tube, and it is shown below:

$$\Delta P_{r,n,\,frict} = F_{PD} . \Delta P_{r,\,frict} \tag{13}$$

Where, F_{PD} is the nanoparticle impact factor and $\Delta P_{r,\,frict}$ is the frictional pressure drop of pure refrigerant. The nanoparticle impact factor is important to correct the frictional pressure drop of pure refrigerant due to nanoparticles suspension. The nanoparticle impact factor was determined by,

$$F_{PD} = \exp\left\{ \phi \times \left[2.19 \times 10^7 \times \frac{d_p}{D_i} + 37.26 \times \frac{\rho_p}{\rho_{l,r}} - 0.63 \times G - 217.73 \times x \times (1 - x) \right] \right\} \tag{14}$$

Where, d_p is the nanoparticle average diameter. A correlation proposed by Müller-Steinhagen and Heck [14] was used to determine the frictional pressure drop of pure refrigerant [8,15]. The model is proposed for two-phase flow with the acceptable vapor quality in range of $0 \le x \le 1$.

$$\Delta P_{r,n,\,frict} = G(1 - x)^{1/3} + bx^3 \tag{15}$$

Where, the factor G is:

$$G = a + 2(b - a)x \tag{16}$$

In equation (16), a and b are frictional pressure gradients for entire flow liquid and the entire flow vapor in the tube which can be determined from:

$$a = f_L \frac{2G^2}{D_i \rho_{r,L}} \tag{17}$$

$$b = f_G \frac{2G^2}{D_i \rho_G} \tag{18}$$

Where, f_L and f_G are the friction factor which depend on Reynolds number; $\rho_{r,L}$ and ρ_G are the density of liquid and vapor refrigerant. The Reynolds number can be calculated from equation (19):

$$\mathrm{Re} = \frac{GD_i}{\mu_r} \tag{19}$$

The friction factor was obtained either from equation (20) or (21) (where appropriate):

$$f = \frac{16}{\mathrm{Re}} \quad \text{for Re < 2000 (laminar flow)} \tag{20}$$

$$f = \frac{0.079}{\mathrm{Re}^{0.25}} \quad \text{for Re} \geq 2000 \text{ (turbulent flow)} \tag{21}$$

3. Result and Discussion

Figure 2 (a) displays the influence of the Al_2O_3 nanoparticle volume fractions on the flow boiling heat transfer coefficient of nanorefrigerant. It was observed that the heat transfer coefficient was proportionally increased according to the particle volume fraction. Formation of molecular adsorption layer on the surface of nanoparticles and the disturbance of nanoparticles reduces the height of boundary layer, which enhances the flow boiling heat transfer coefficient of nanorefrigerant [9]. Figure 2 (b) shows the flow boiling heat transfer coefficient of Al_2O_3/R141b nanorefrigerant as a function of vapor quality. The highest heat transfer coefficient found at vapor quality of 0.2 where the value was 1755.82 kW/m^{2}K with 5 vol. % of particle concentration and heat transfer coefficient of pure refrigerant with same vapor quality was only 1.22 kW/m^{2}K. The lowest heat transfer coefficient was found 4.68 kW/m^{2}K at vapor quality of 0.3 with 1 vol. % of particle concentration. Even with only 1 vol. %, the minimum heat transfer coefficient enhancement was 383 % relative to pure R141b refrigerant.

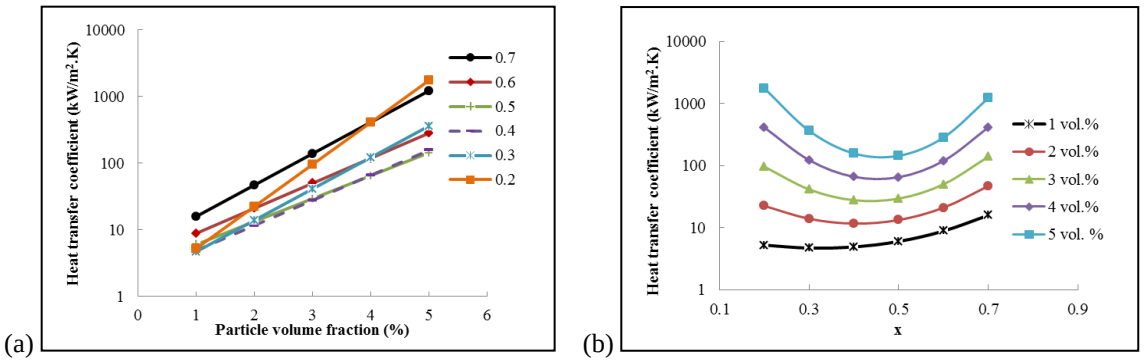

Fig. 2. (a) Flow boiling heat transfer coefficient as a function of particle volume concentration at different vapour quality (from 0.2 to 0.7); (b) Flow boiling heat transfer coefficient as a function of vapour quality for different particle volume concentrations (from 1 to 5 vol. %).

Figure 3 (a) and (b) shows the pressure drop characteristics of Al_2O_3/R141b nanorefrigerant as a function of nanoparticle volume concentration and vapor quality, respectively. The highest frictional pressure drop occurred at vapor quality of 0.7 where the value was 464.27 kPa with 5 vol. % of particle concentration and pressure drop of pure refrigerant with same vapor quality was only 5.5 kPa. The lowest pressure drop was found 3.34 kPa at vapor quality of 0.2 with 1 vol. % of particle concentration. Even with only 1 vol. %, the pressure drop enhancement was 181 % relative to pure R141b refrigerant. Suspending nanoparticles into the refrigerant generally increase the pressure drop even though the mass flow

rate of the refrigerant was considered to be constant in this study. When the particle volume fraction was suspended more than 3 vol. %, the enhancements of pressure drop for all vapor qualities were found to increase rapidly. By increasing the nanoparticles concentration, more collision between the nanoparticles and wall interaction could be occurred and higher pressure drop compared to pure refrigerant was observed for the nanorefrigerant.

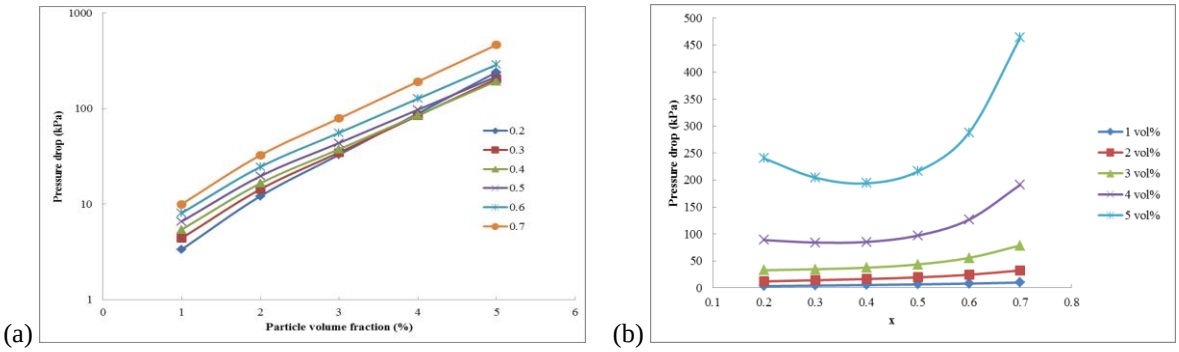

Fig. 3. (a) Frictional pressure drop as a function of particle volume concentrations at different vapour quality (from 0.2 to 0.7); (b) Frictional pressure drop as a function of vapour quality for different particle volume concentrations (from 1 to 5 vol. %).

Conclusion

In this study, attempt was made to investigate the flow boiling heat transfer coefficient and frictional pressure drop characteristics of Al_2O_3/R141b nanorefrigerants. Throughout this study it was found that volume fractions have significant effects over heat transfer and pressure drop characteristics of nanorefrigerant.

Due to significant enhancement of boiling heat transfer coefficient, nanorefrigerants could be implemented in refrigeration systems but an optimum particle volume fraction is needed to avoid the high pressure drop as well as pumping power.

Moreover, more experimental investigation is needed to implement nanorefrigerants in refrigeration systems. It is noteworthy that, there will be some unknown effects on the compressor performance of the refrigeration or air-conditioning system. Nevertheless the present study would hopefully help the researchers working in this area to carry out some experimental studies.

Acknowledgements

The authors acknowledge the financial support from High Impact Research Grant (HIRG) fund under UM-MoHE (Project no. UM.C/HIR/MoHE/ENG/40).

References

[1] Peng, H., Ding, G., Hu, H., 2011. Influences of refrigerant-based nanofluid composition and heating condition on the migration of nanoparticles during pool boiling. Part I: Experimental measurement, International Journal of Refrigeration 34, p. 3770.

[2] Wang, K., Ding, G., Jiang, W., 2005. "Development of nanorefrigerant and its rudiment property,"- 8th International Symposium on Fluid Control, Measurement and Visualization, Chengdu, China: China Aerodynamics Research Society.

[3] Mahbubul, I.M., Fadhilah, S.A., Saidur, R., Leong, K.Y., Amalina, M.A., 2012. Thermophysical properties and heat transfer performance of Al_2O_3/R-134a nanorefrigerants, International Journal of Heat and Mass Transfer [HMT9361; DOI: 10.1016/j.ijheatmasstransfer.2012.10.007].

[4] Jiang, W., Ding, G., Peng, H., 2009. Measurement and model on thermal conductivities of carbon nanotube nanorefrigerants, International Journal of Thermal Sciences 48, p. 1108.

[5] Park, K., Jung, D., 2007. Boiling heat transfer enhancement with carbon nanotubes for refrigerants used in building air-conditioning, Energy and Buildings 39, p. 1061.

[6] Kedzierski, M.A., 2011. Effect of Al_2O_3 nanolubricant on R134a pool boiling heat transfer, International Journal of Refrigeration 34, p. 498.

[7] Henderson, K., Park, Y-G., Liu, L., Jacobi, A.M., 2010. Flow-boiling heat transfer of R-134a-based nanofluids in a horizontal tube, International Journal of Heat and Mass Transfer 53, p. 944.

[8] Ould Didi, M., Kattan, N., Thome, J., 2002. Prediction of two-phase pressure gradients of refrigerants in horizontal tubes, International Journal of Refrigeration 25, p. 935.

[9] Peng, H., Ding, G., Jiang, W., Hu, H., Gao, Y., 2009. Measurement and correlation of frictional pressure drop of refrigerant-based nanofluid flow boiling inside a horizontal smooth tube, International Journal of Refrigeration 32, p. 1756.

[10] Lemmon, E.W., McLinden, M.O., Huber, M.L., 2002. NIST Reference Fluid Thermodynamic and Transport Properties—Refprop 7.0, NIST Std, in Database: Boulder.

[11] Peng, H., Ding, G., Jiang, W., Hu, H., Gao, Y., 2009. Heat transfer characteristics of refrigerant-based nanofluid flow boiling inside a horizontal smooth tube, International Journal of Refrigeration 32, p. 1259.

[12] Saitoh, S., Daiguji, H., Hihara, E., 2007. Correlation for boiling heat transfer of R-134a in horizontal tubes including effect of tube diameter, International Journal of Heat and Mass Transfer 50, p. 5215.
[13] Dittus, F., Boelter, L., 1930. Heat Transfer In Automobile Radiators of the Tubuler Type, University of California Publications in Engineering 2, p. 443.
[14] Müller-Steinhagen, H., Heck, K., 1986. A simple friction pressure drop correlation for two-phase flow in pipes. Chemical Engineering and Processing 20, p. 297.
[15] Mahbubul, I.M., Saidur, R., Amalina, M.A., 2012. Investigation of viscosity of R123-TiO_2 nanorefrigerant, International Journal of Mechanical and Materials Engineering 7, p. 146.

Available online at www.sciencedirect.com

SciVerse ScienceDirect

Procedia Engineering 00 (2012) 000–000

Procedia Engineering

www.elsevier.com/locate/procedia

5th BSME International Conference on Thermal Engineering

Heat Transfer Enhancement of Nanofluids in a Lid-Driven Triangular Enclosure Having a Discrete Heater

M. M. Billah[a,c,*], M. M. Rahman[b], U. M. Sharif[c]

[a]*Department of Arts and Sciences, Ahsanullah University of Science and Technology (AUST), Dhaka–1208, Bangladesh*
[b]*Department of Mathematics, Bangladesh University of Engineering and Technology (BUET), Dhaka–1000, Bangladesh*
[c]*Department of Mathematics, Jahangirnagar University (JU), Savar, Dhaka–1342, Bangladesh*

Abstract

In the present study, the behaviour of nanofluids is investigated numerically in a lid-driven triangular enclosure which has a partially heated on bottom side to gain insight into convective recirculation and flow processes induced by a nanofluid. The present model is developed to examine the behaviour of nanofluids taking into account the heater length. Fluid mechanics and conjugate heat transfer, described in terms of continuity, linear momentum and energy equations, were predicted by using the Galerkin finite element method. Comparisons with previously published work on the basis of special cases are performed and found to be in excellent agreement. Numerical results are obtained for a wide range of parameters such as the Richardson number, and heater length. Copper-water nanofluids is used with Prandtl number, Pr = 6.2. The streamlines, isotherm plots and the variation of the average Nusselt number at the hot surface as well as average fluid temperature in the enclosure is presented and discussed in detailed.

Keywords: Penalty finite element method; nanofluid; lid-driven triangular enclosure; partial heater.

Nomenclature

c_p	Specific heat at constant pressure	v	vertical velocity component (ms^{-1})
g	gravitational acceleration (ms^{-2})	Y	dimensionless vertical coordinate
Gr	Grashof number		
H	enclosure height (m)	Greek symbols	
HL	Heater length (m)	α	thermal diffusivity (m^2s^{-1})
k	thermal conductivity ($Wm^{-1}K^{-1}$)	β	thermal expansion coefficient (K^{-1})
L	length of the cavity (m)	δ	solid volume fraction
Nu	Nusselt number	μ	dynamic viscosity (kg $m^{-1}s^{-1}$)
p	dimensional pressure (Nm^{-2})	υ	kinematic viscosity (m^2s^{-1})
P	dimensionless pressure	θ	non-dimensional temperature
Pr	Prandtl number	ρ	density (kg m^{-3})
Re	Reynolds number	γ	penalty parameter
Ri	Richardson number	Γ	general dependent variable
T	temperature (K)	Θ	average temperature
u	horizontal velocity component (ms^{-1})		

* Corresponding author. Tel.: +88-01715400423; fax: +880-2-9860564.
E-mail address: mmb.edu@gmail.com/ mmb.as@aust,edu

U	dimensionless horizontal velocity component	Subscripts	
V	dimensionless vertical velocity component	h	hot
V_0	lid velocity (ms^{-1})	c	cold
$\overline{V}$	cavity volume (m^3)	f	fluid
x	horizontal coordinate (m)	nf	nanofluid
X	dimensionless horizontal coordinate	s	Solid nanoparticle
y	vertical coordínate (m)		

1. Introduction

The heat transfer properties of thermo fluid play an important role in the development of energy-efficient heat transfer equipment. Passive enhancement methods are commonly utilized in the electronics and transportation devices. But the working fluids such as ethylene glycol, water and engine oil have poor heat transfer properties. In that regard, various techniques have been proposed to enhance the heat transfer performance of fluids. Researchers have also tried to increase the thermal conductivity of base fluids by suspending micro- or larger-sized solid particles in fluids since the thermal conductivity of solid is typically higher than that of liquids. Therefore a new class of heat transfer fluids can be designed by suspending metallic nanoparticles in conventional heat transfer fluids. In recent years, nanofluids have attracted more attention for cooling in various industrial applications such as Silicon Mirror Cooling, electronics cooling, vehicle cooling, transformer cooling, nuclear reactors, lakes and reservoirs, and solar applications etc.

A detailed explanation of the transient hot wire method in measuring the thermal conductivity of nanofluids is given by Lee et al. [1]. Maiga et al. [2] performed numerical simulations to study the convective heat transfer in nanofluids by assuming the nanofluid as a single phase fluid. Roy et al.[3] conducted a numerical study of heat transfer for Al_2O_3/water nanofluids in a radial cooling system. Xuan et al.[4] for the first time proposed a Lattice Boltzmann model for simulating flow and energy transport processes inside nanofluids. Xue et al. [5] were first to use molecular dynamics simulation to identify the effect of liquid layering at the liquid-solid interface on thermal transport in nanofluids. He et al. [6] studied the convective heat transfer of TiO_2 nanofluids under the laminar conditions using an Eulerian-Lagrangian two-phase model. Wen and Ding [7] investigated the effect of particle migration on heat transfer in suspensions of nanoparticles flowing through mini channels. Rahman et al.[8] made a numerical investgation of heat transfer enhancement of nanofluids in an inclined lid-driven triangular enclosure. Billah et al.[9] conducted a numerical analysis on heat transfer enhancement of copper–water nanofluids in an inclined lid-driven triangular enclosure.

2. Mathematical Formulation

The physical model for the present study is sketched in Fig. 1. The problem deals with a steady two-dimensional flow of nanofluid contained in a lid-driven triangular enclosure. The length of the base wall and height of the sliding wall of the enclosure are denoted by L and H, respectively. The sliding wall of the cavity is kept adiabatic and allowed to move from bottom to top at a uniform speed V_0. In addition, the temperature (T_h) of the bottom wall is higher than the temperature (T_c) of the right inclined wall.

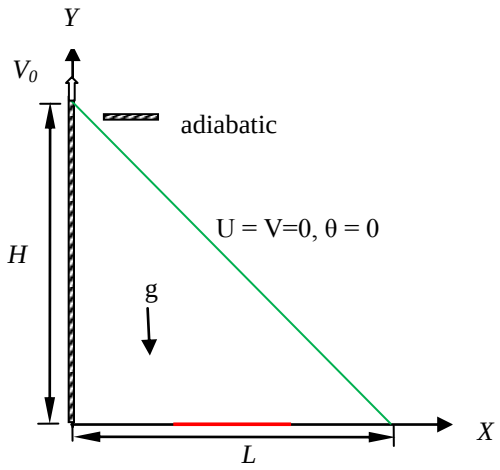

Fig. 1. Schematic of the problem with the domain and boundary

The free space in the enclosure is filled with copper water nanofluids. The nanofluid in the enclosure is Newtonian, incompressible and laminar. The nanoparticles are assumed to have uniform shape and size. It is assumed that thermal equilibrium exists between the base fluid and nanoparticles, and no slip occurs between the two media. The physical properties of the nanofluid are considered to be constant except the density variation in the body force term of the momentum equation which is satisfied by the Boussinesq's approximation. Under the above assumptions, the system of equations governing the two-dimensional motion of a nanofluid is as follows:

$$\frac{\partial u}{\partial x}+\frac{\partial v}{\partial y}=0 \tag{1}$$

$$u\frac{\partial u}{\partial x}+v\frac{\partial u}{\partial y}=-\frac{1}{\rho_{nf}}\frac{\partial p}{\partial x}+\frac{\mu_{nf}}{\rho_{nf}}\left(\frac{\partial^2 u}{\partial x^2}+\frac{\partial^2 u}{\partial y^2}\right) \tag{2}$$

$$u\frac{\partial v}{\partial x}+v\frac{\partial v}{\partial y}=-\frac{1}{\rho_{nf}}\frac{\partial p}{\partial y}+\frac{\mu_{nf}}{\rho_{nf}}\left(\frac{\partial^2 v}{\partial x^2}+\frac{\partial^2 v}{\partial y^2}\right)+\frac{(\rho\beta)_{nf}}{\rho_{nf}}(T-T_c)g \tag{3}$$

$$u\frac{\partial T}{\partial x}+v\frac{\partial T}{\partial y}=\alpha_{nf}\left(\frac{\partial^2 T}{\partial x^2}+\frac{\partial^2 T}{\partial y^2}\right) \tag{4}$$

The effective density ρ_{nf} of the nanofluid is defined by

$$\rho_{nf}=(1-\delta)\rho_f+\delta\rho_s \tag{5}$$

where δ is the solid volume fraction of nanoparticles. In addition, the thermal diffusivity α_{nf} of the nanofluid can be expressed as:

$$\alpha_{nf}=\frac{k_{nf}}{(\rho c_p)_{nf}} \tag{6}$$

The heat capacitance of nanofluids can be defined as:

$$(\rho c_p)_{nf}=(1-\delta)(\rho c_p)_f+\delta(\rho c_p)_s \tag{7}$$

Additionally, $(\rho\beta)_{nf}$ is the thermal expansion coefficient of the nanofluid and it can be determined by

$$(\rho\beta)_{nf}=(1-\delta)(\rho\beta)_f+\delta(\rho\beta)_s \tag{8}$$

Furthermore, μ_{nf} is the dynamic viscosity of the nanofluid introduced by Brikman [10] as

$$\mu_{nf}=\frac{\mu_f}{(1-\delta)^{2.5}} \tag{9}$$

The effective thermal conductivity of nanofluid was intoduced by Kanafer et al.[11] as:

$$\frac{k_{nf}}{k_f}=\frac{k_s+2k_f-2\delta(k_f-k_s)}{k_s+2k_f+\delta(k_f-k_s)} \tag{10}$$

where, k_s is the thermal conductivity of the nanoparticles and k_f is the thermal conductivity of base fluid.
Introducing the following dimensionless variables

$$X=\frac{x}{L},\ Y=\frac{y}{L},\ U=\frac{u}{V_0},\ V=\frac{v}{V_0},\ P=\frac{(p+\rho gy)L^2}{\rho_{nf}V_0{}^2},\ \theta=\frac{(T-T_c)}{(T_h-T_c)} \tag{11}$$

The governing equations may be written in the dimensionless form as

$$\frac{\partial U}{\partial X}+\frac{\partial V}{\partial Y}=0 \tag{12}$$

$$U\frac{\partial U}{\partial X}+V\frac{\partial U}{\partial Y}=-\frac{\partial P}{\partial X}+\frac{1}{Re}\frac{\rho_f}{\rho_{nf}}\frac{1}{(1-\delta)^{2.5}}\left(\frac{\partial^2 U}{\partial X^2}+\frac{\partial^2 U}{\partial Y^2}\right)+ \tag{13}$$

$$U\frac{\partial V}{\partial X}+V\frac{\partial V}{\partial Y}=-\frac{\partial P}{\partial Y}+\frac{1}{Re}\frac{\rho_f}{\rho_{nf}}\frac{1}{(1-\delta)^{2.5}}\left(\frac{\partial^2 V}{\partial X^2}+\frac{\partial^2 V}{\partial Y^2}\right)+\frac{(\rho\beta)_{nf}}{\rho_{nf}\beta_f}Ri\,\theta \tag{14}$$

$$U\frac{\partial\theta}{\partial X}+V\frac{\partial\theta}{\partial Y}=\frac{\alpha_{nf}}{\alpha_f}\frac{1}{Re\,Pr}\left(\frac{\partial^2\theta}{\partial X^2}+\frac{\partial^2\theta}{\partial Y^2}\right) \tag{15}$$

The nondimensional numbers that appear in equations (13)-(15) are as follows:

Reynolds number $Re=V_0L/\upsilon_f$, Prandtl number $Pr=\nu_f/\alpha_f$ and Richardson number $Ri=g\beta_f\left(T_h-T_c\right)L/V_0^2$

The appropriate boundary conditions for the governing equations are

on the bottom wall: $U=V=0,\ \theta=1$ (on the heater), $U=V=0,\ \frac{\partial\theta}{\partial N}=0$ (on the unheated part)

on the left wall: $U=0, V=1,\ \frac{\partial\theta}{\partial N}=0$

on the right inclined wall: $U=V=0,\ \theta=0$

where N is the non-dimensional distances either X or Y direction acting normal to the surface.

The average Nusselt number at the heated surface of the cavity may be expressed as

$$Nu=-\frac{k_{nf}}{k_f}\int_0^1\frac{\partial\theta}{\partial Y}dX \tag{16}$$

and average fluid temperature in the enclosure may be defined as $\Theta=\int\theta\,d\overline{V}/\overline{V}$ (17)

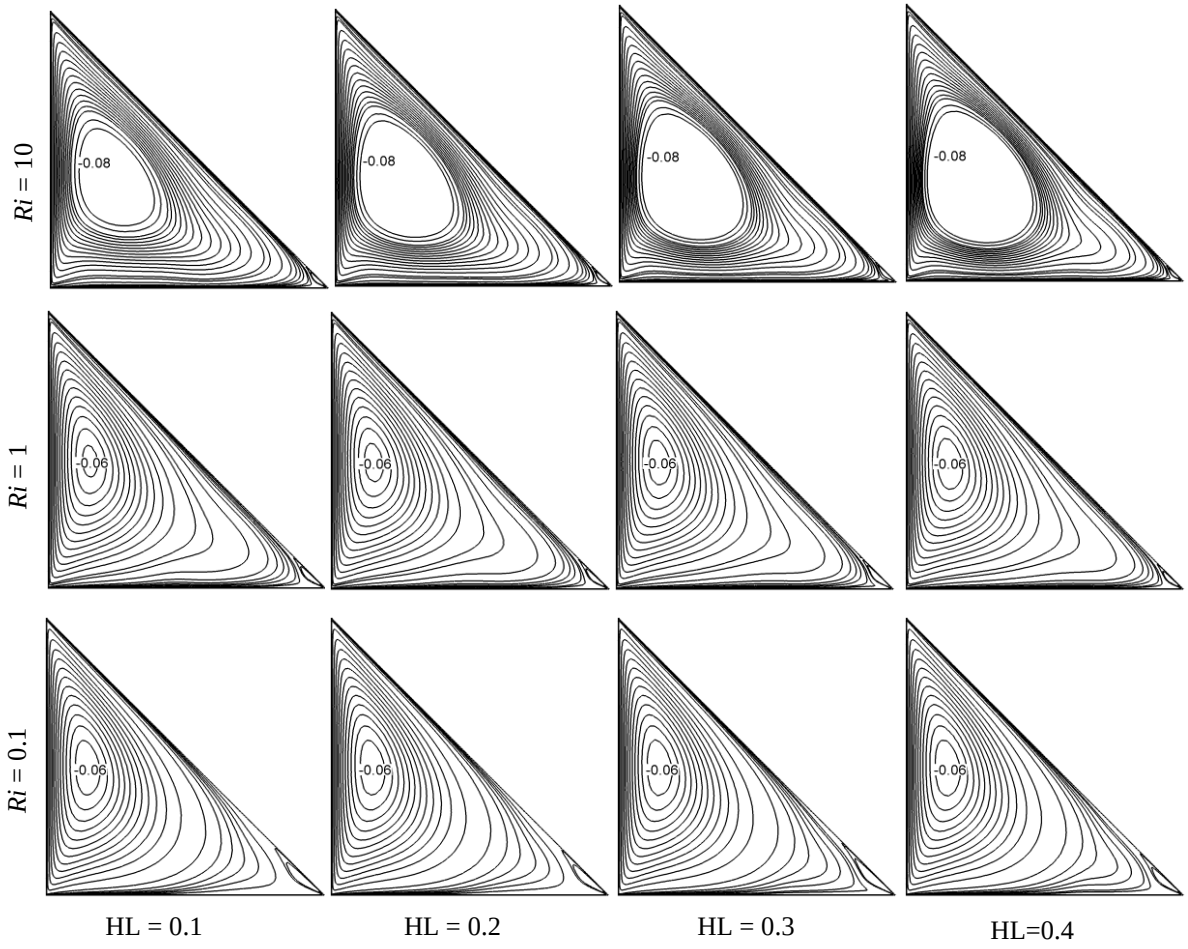

Fig. 2. Effects of heater length on streamlines at different *Ri*

3. Solution Procedure

The Galerkin weighted residual method of finite element formulation is employed as a numerical scheme. The finite element method begins by the partition of the continuum area of interest into a number of simply shaped regions known as elements. These elements may be different shapes and sizes. Within each element, the dependent variables are approximated using interpolation functions. In the present study erratic grid size system is considered especially near the walls to capture the rapid changes in the dependent variables. The coupled governing equations (12)-(15) are transformed into sets of algebraic equations using finite element method to reduce the continuum domain into discrete triangular domains. The system of algebraic equations is solved by iteration technique. The solution process is iterated until the subsequent convergence condition is satisfied: $\left|\Gamma^{m+1}-\Gamma^{m}\right|\leq 10^{-6}$ where m is number of iteration and Γ is the general dependent variable.

4. Results and Discussion

The present numerical study is carried out for copper-water nanofluids as working fluid with Prandtl number of 6.2. In this investigation, our attention is taken into account to investigate the effects of controlling parameters namely the heater length (*HL*), and Richardson number (*Ri*). It is worth to note that the value of *Ri* is varied from 0.1 to 10 by changing Grashof number *Gr* to cover forced convection dominated region, pure mixed convection and free convection dominated region. Moreover, the results of this study are presented in terms of streamlines and isotherms. Furthermore, the heat transfer effectiveness of the enclosure is displayed in terms of average Nusselt number *Nu* and the dimensionless average bulk temperature Θ.

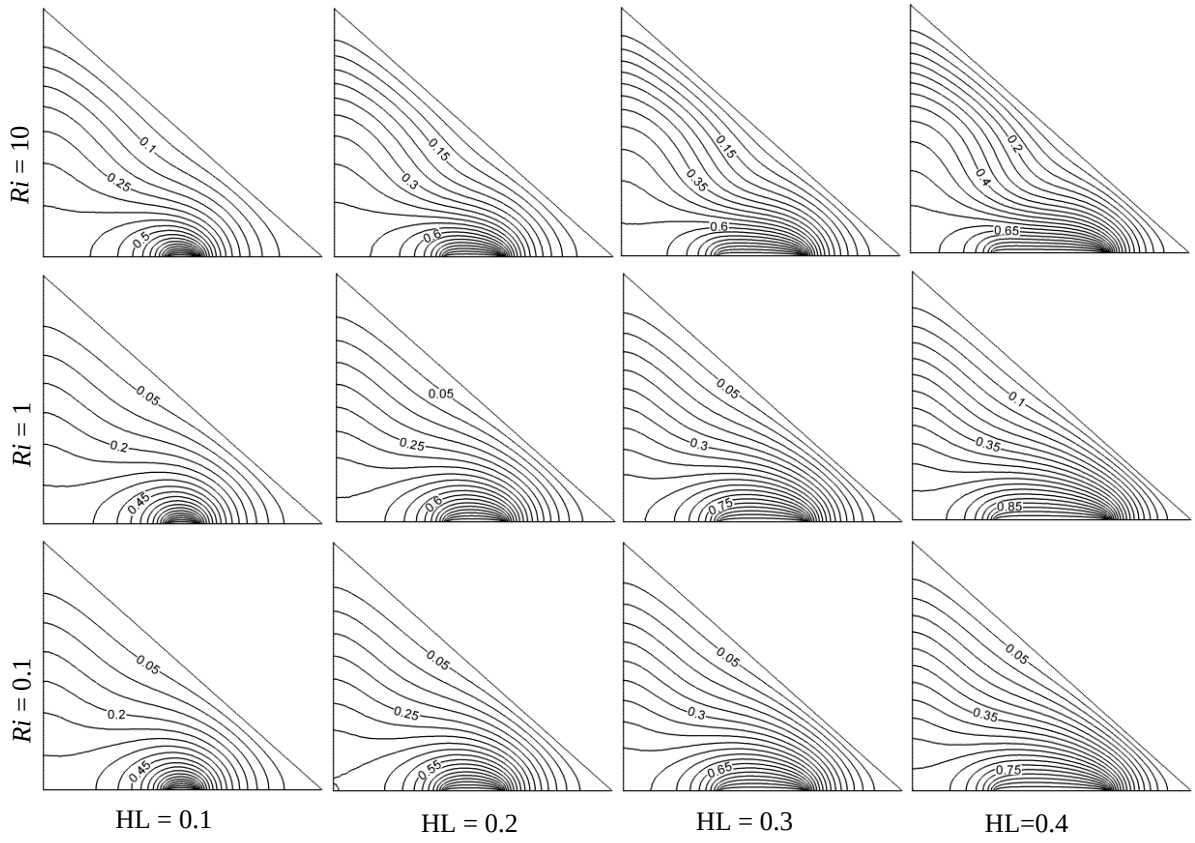

Fig. 3. Effects of heater length on isotherm at different *Ri*

Fig. 2 shows the streamlines in a lid-driven triangular enclosure for four heater lengths *HL*(= 0.1, 0.2, 0.3, and 0.4) at *Ri* =(0.1, 1 and 10). The fluid flow in a 2-D lid-driven enclosure is characterized by a primary clockwise circulating cell near the vicinity of the sliding wall in the enclosure generated by the motion of the lid and a weaker anticlockwise rotating cell near the right bottom corner for *Ri* = 0.1 and 1. In addition, the main cell is generated by the lid dragging the neighboring fluid. Though the flow strength of the main cell is same, the size of the main cell is affected for changing *Ri* from 0.1 to 1. One may notice that the flow strength of the main cell changes from -0.06 to -0.08 while *Ri* increases from 1 to 10. It is also found from the streamlines that the size of clockwise rotating cell is increasing when *HL* is increasing for Ri = 10, and

dramatically the weaker anticlockwise rotating cell disappears. This is due to increase in the heater length as a result of high-energy transport through the flow associated with the irregular motion of the ultrafine particles. The isotherm plots indicate the lines with equal intervals between unity (hot wall) and zero (cold wall). Fig. 3 illustrates the streamlines in a lid-driven triangular enclosure for four heater lengths *HL*(= 0.1, 0.2, 0.3, and 0.4) at *Ri* =(0.1, 1 and 10). It is noticed that isotherm lines become denser towards the heater for each value of *HL* at the considered value of *Ri*. It is also observed that the thermal layer become thicker gradually towards the heated surface of the enclosure for the increasing value of *Ri*, which indicates the steeper temperature gradient in the horizontal direction in this region. At the upper part of the cavity, the temperature gradients are very small due to the mechanically-driven circulations.

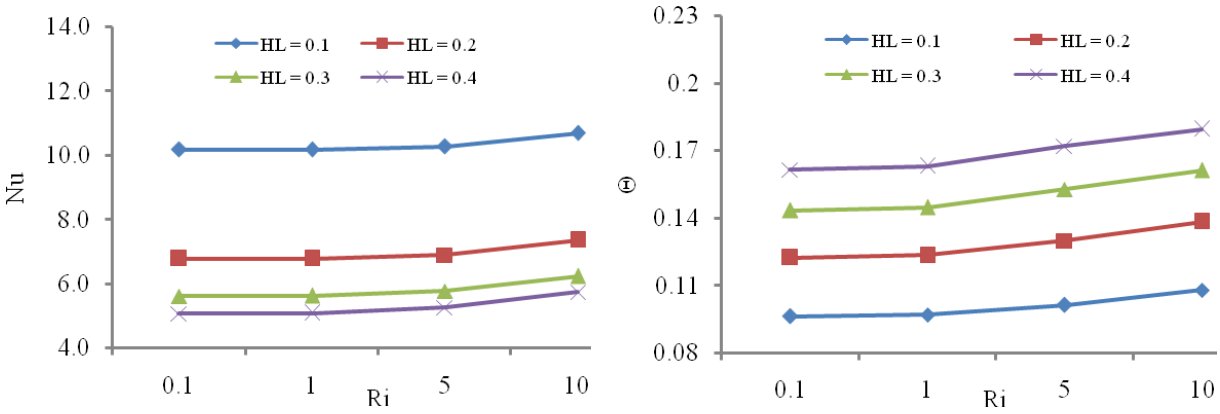

Fig. 4. Effects of average Nusselt (left) and average temperature (right) for different *Ri*

Fig.4 plots the average Nusselt number (*Nu*) at the hot surface, which is a measure of the overall heat transfer rate as a function of Richardson number for the abovementioned values of heater length. As clearly be seen that *Nu* increases very slowly for all values of heater length with the increasing *Ri*. However, the values of *Nu* are always higher for the lowest value of *HL* (= 0.1). It is found that heat transfer increased by 100% as *HL* decreases from 0.4 to 0.1 at *Ri* =1. The effect of heater length on average fluid temperature (Θ) in the enclosure is exposed in right column of Fig. 4. It is observed that Θ increases significantly with the increasing *Ri* for all values of heater length. It is noticed that Θ is maximum for the smallest values HL (= 0.1).

5. Conclusion

Mixed convection in a lid-driven triangular enclosure filled with nanofluids is studied numerically. Results for various parametric conditions are presented and discussed. From the above study, the following conclusions are made:

- The flow and thermal fields as well as the heat transfer rate inside the enclosure are strongly dependent on the Richardson number.
- Maximum heat transfer occurs when heater is small in size.
- Nanofluids are capable to modify the flow pattern.
- The heater length is a good control parameter for both pure and nanofluid filled enclosures

References

[1] Lee, S., Choi, S.U.S., Li, S., Eastman, J.A., 1999. Measuring Thermal Conductivity of Fluids Containing Oxide Nanoparticles, Journal of Heat Transfer 121, p. 280.

[2] Maiga, S.E.B., Palm, S.J., Nguyen, C.T., Roy, G., Galanis, G., 2005. Heat transfer enhancement by using nanofluids in forced convection flows, International Journal of Heat Fluid Flow 26, p.530.

[3] Roy, G., Nguyen, C.T., Lajoie, P.R., 2004. Numerical investigation of laminar flow and heat transfer in a radial flow cooling system with the use of nanofluids, Superlatt. Microstruct 35, p. 497.

[4] Xuan, Y., Yu, K, Li, Q.,2005. Investigation on flow and heat transfer of nanofluids by the thermal Lattice Boltzmann model, Progress in Computational Fluid Dynamics 5, P.13.

[5] Xue, L., Keblinski, P., Phillpot, S.R., Choi, S.U.S., Eastman, J.A., 2004. Effect of liquid layering at the liquid–solid interface on thermal transport, International Journal of Heat and Mass Transfer 47, p. 4277.

[6] He, Y., Men, Y., Zhao, Y., Le, H., Ding, Y., 2009. Numerical investigation into the convective heat transfer of TiO_2 nanofluids flowing through a straight tube under the laminar flow conditions, Applied Thermal Engineering 29, p.1965.
[7] Wen, D., Ding, Y., 2005. Effect of particle migration on heat transfer in suspensions of nanoparticles flowing through mini channels. Microfluid Nanofluid, DOI 10.1007/s, p.183.
[8] Rahman, M.M., Billah, M.M., Rahman, ATMM., Kalam, M.A., Ahsan, A., 2011, Numerical investgation of heat transfer enhancement of nanofluids in an inclined lid-driven triangular enclosure, International Communications in Heat and Mass Transfer 38, p.1360.
[9] Billah, M.M., Rahman, M.M., Shahabuddin, M., Azad, A.K., 2011. Heat transfer enhancement of copper–water nanofluids in an inclined lid-driven triangular enclosure, Journal of Scientific Research.3,p.525.
[10] Brinkman, H.C,. 1952. The viscosity of concentrated suspensions and solutions, Journal of Chemical Physics 20, p. 571.
[11] Khanafer, K., Vafai, K., Lightstone, M., 2003. Buoyancy-driven heat transfer enhancement in a two-dimensional enclosure utilizing nanofluids, International Journal of Heat and Mass Transfer 46, p. 3639.

Available online at www.sciencedirect.com

SciVerse ScienceDirect

Procedia Engineering 00 (2012) 000–000

Procedia Engineering

www.elsevier.com/locate/procedia

5th BSME International Conference on Thermal Engineering

Cooling of Microchannel Heat Sinks with Gaseous Coolants

Ahmed Mohammed Adham[a]*, Normah Mohd-Ghazali[b], Robiah Ahmad[c]

[a,b]*Universiti Teknologi Malaysia, Faculty of Mechanical Engineering, Johor Bahru, Skudai 81310, Malaysia*
[c]*Universiti Teknologi Malaysia, International campus, Razak School of Engineering and Advanced Technology, Kuala Lumpur 54100,Malaysia*

Abstract

In this paper, the optimization of the cooling performance of a rectangular microchannel heat sink is investigated with four different gaseous coolants; air, ammonia gas, dichlorodifluoromethane (R-12) and chlorofluoromethane (R-22). A systematic robust thermal resistance model together with a methodical pumping power calculation is used to formulate the objective functions, the thermal resistance and pumping power. The non-dominated sorting genetic algorithm (NSGA-II), a multi-objective algorithm, is applied in the optimization procedure. The optimized thermal resistances obtained are 0.178, 0.14, 0.08 and 0.133°K/W for the pumping powers of 6.4, 4, 22.4 and 16.5 W for air, ammonia gas, R-12 and R-22, respectively. These results show that among all the gaseous coolants investigated in the current study, ammonia gas exhibited balanced thermal and hydrodynamic performances. Due to the Montreal Protocol, the coolant R-12 is no longer produced while R-22 will eventually be phased out. The results from ammonia provide a strong motivation to conduct more investigations on the potential usage of this gaseous coolant in the electronic cooling industry.

Keywords: Microcahnnel; Gaseous coolants; Thermal resistance; Optimization.

Nomenclature

A_{eff}	effective area available for heat transfer (m^2)
A_{hs}	heat sink cross sectional area (m^2)
A_t	induction tubes cross sectional area (m^2)
Cp	specific heat (J/kg.K)
D_h	hydraulic diameter (m)
f	friction factor
H	heat sink height (m)
H_c	channel height (m)
G	volumetric flow rate (l/s)
h_{av}	average heat transfer coefficient ($W/m^2.K$)
k	thermal conductivity (W/m.K)
L	Heat sink length (m)
Nu	Nusselt number
n	number of microchannels
Δp	pressure drop (mbar)
Δp_{tu}	tube pressure drop (mbar)
q	heat flux (W/m^2)

* Corresponding author. Tel.: +60123398728; fax: +60326934844.
E-mail address: maahmed4@live.utm.my; ahamedadhm@yahoo.com.

Re	Reynolds number
R	thermal resistance (K/W)
W	heat sink width (m)
w_c	channel width (m)
w_w	wall (fin) width (m)
V_{mf}	velocity inside the channels (m/s)
V_{mt}	velocity inside the tubes (m/s)
P_p	pumping power (W)
Greek symbols	
α	channel aspect ratio
β	fin spacing ratio
ρ	density (kg/m^3)
μ	dynamic viscosity (kg/m.s)
η	fin efficiency
Subscripts	
hs	Heat sink
tu,t	tube
tot	total
f	fluid (coolant)
w	wall

1. Introduction

With the enormous development in the capabilities of the microelectronic mechanical systems (MEMS), the use of the microchannel heat sink has acquired great importance because it provides a high heat dissipation rate, compatibility with the small allowable space and ultimately a low manufacturing cost. Liquid coolants have been extensively used with the microchannel heat sinks for their high capabilities of absorbing heat. However, the associated issues of the high pumping power demands [1,2], leakage [3], and passage clogging [4] in the case of the nanofluids usage, have not been fully addressed. Air was used as an alternative coolant in many microchannel heat sink systems [5-7]. However, its poor heat removal capabilities [8] have limited its applications. In this study, the overall performance of the microchannel heat sink using several gaseous coolants is investigated. The coolants are air, ammonia gas, R-12 and R-22. The search for an alternative coolant to overcome the difficulties of the liquid coolants was the motivation to consider these gaseous coolants. An optimization scheme which incorporates the thermal resistance model as an objective functions formulator and the non-dominated sorting genetic algorithm (NSGA-II) as an optimization performer is employed to investigate the overall performance of the considered system under these different gaseous coolants.

2. Mathematical model

Figure 1 illustrates the schematic drawing of the rectangular microchannel heat sink under investigation in the current study.

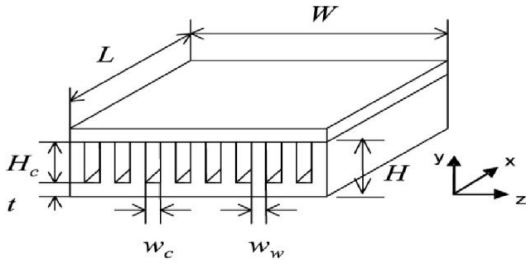

Fig. 1. Schematic drawing of the microchannel heat sink.

The microchannel heat sink comprised of n number of microchannels attached to each other with an adiabatic covering plate bonded on top to close the microchannels. Induction tubes are used to transport the coolant to and from the microchannels to avoid the bypass flow and to provide a sufficient length for the flow to reach the fully develop status. The above mentioned microchannel system performance is evaluated using a systematic thermal resistance model and a methodical pumping power calculation. The approach offered by Wen and Choo [9] and Kleiner et al. [10] to evaluate the

total thermal resistance and pumping power are followed and modified where needed. Kleiner et al. [10] model was used because it was experimentally verified and it showed superior thermal and hydrodynamic performance compared to the previous conventional air-cooled microchannel heat sink systems.

2.1. Thermal performance model

The thermal performance of a microchannel heat sink is evaluated through its total thermal resistance. The total thermal resistance of any heat sink is described as the ratio of the temperature difference between the maximum temperature of the substrate and the coolant inlet temperature, to the heat flux. The maximum temperature is normally located at the end of the microchannels and the heat flux is assumed to be uniformly applied to the back side of the microchannel heat sink. The total thermal resistance of the heat sink is given by:

$$R_{tot} = \frac{T_{surf,\max} - T_{in}}{q} \tag{1}$$

where $T_{surf,max}$ and T_{in} are the highest and the inlet temperatures of the substrate and the coolant, respectively. Eqn. (1) can be expressed in terms of the dominated components of the total thermal resistance,

$$R_{tot} = R_{conv} + R_{capa} \tag{2}$$

where R_{conv} and R_{capa} are the convective and capacitive thermal resistances, respectively. The first term in Eqn. (2) can be expressed as,

$$R_{conv} = \frac{1}{h_{av} A_{eff}} \tag{3}$$

The effective area for heat transfer in Eqn. (3) can be defined as,

$$A_{eff} = nL(w_c + 2\eta H_c) \tag{4}$$

The number of the microchannels and the fin efficiency are calculated according to the following equations,

$$n = \frac{W}{w_w + w_c} \tag{5}$$

$$\eta = \frac{\tanh(mH_c)}{mH_c} \tag{6}$$

where m is the fin parameter given by,

$$m = \sqrt{\frac{2h_{av}}{k_w w_w}} \tag{7}$$

where k_w is the thermal conductivity of the heat sink material which is assumed to be made of aluminum. The second term in Eqn. (2) is the capacitive thermal resistance which can be expressed as,

$$R_{capa} = \frac{1}{\rho_f cp_f G} \tag{8}$$

$$G = nH_c w_c V_{mf} \tag{9}$$

The convective and capacitive thermal resistance expressions are further simplified using the channel aspect ratio (α) and the fin spacing ratio (β) along with several other auxiliary equations as follows,

$$\alpha = \frac{H_c}{w_c} \tag{10}$$

$$\beta = \frac{w_w}{w_c} \tag{11}$$

$$D_h = \frac{2}{1+\alpha} H_c \tag{12}$$

$$\mathrm{Re} = \frac{2\rho_f G}{\mu_f n H_c} \frac{\alpha}{1+\alpha} \tag{13}$$

$$Nu = \frac{h_{av} 2H_c}{k_f (\alpha+1)} \tag{14}$$

Substituting Eqns. (10-14) into Eqns. (3, 8) results in the final expression of the total thermal résistance as,

$$R_{tot} = \frac{L}{cp_f \mu_f} \frac{2}{\mathrm{Re}} \frac{1+\beta}{1+\alpha} + \frac{1}{h_{av}} \frac{1+\beta}{1+2\alpha\eta} \tag{15}$$

The average heat transfer coefficient appearing in Eqn. (15) is evaluated using the Nusselt number correlation given by Kim and Kim [11] for a laminar fully developed flow,

$$Nu = 2.253 + 8.164 \left(\frac{\alpha}{1+\alpha}\right)^{1.5} \tag{16}$$

2.2. Hydrodynamic performance model

In the current study, the hydrodynamic performance of the microchannel heat sink is assessed using a pressure drop calculation and the associated required pumping power. The methodology offered by Kleiner et al. [10] where induction tubes are employed to transfer the coolant is used and modified. The total pressure drop is given by,

$$\Delta p_{tot} = \Delta p_{hs} + \Delta p_{tu} \tag{17}$$

where Δp_{tot} , Δp_{hs} and Δp_t are the total, heat sink and tubes pressure drops, respectively. The pressure drop [10] inside the microchannel is modified and the final expression for the total pressure drop is

$$\Delta p_{tot} = f_{hs} \frac{L}{D_h} \rho_f \frac{V_{mf}^2}{2} + (1.79 - 2.32(\frac{1}{1+\beta}) + 0.53(\frac{1}{1+\beta})^2) \rho_f \frac{V_{mf}^2}{2} + f_{t1} \frac{L_{t1}}{D_{tu}} \rho_f \frac{V_{mt}^2}{2} + f_{t2} \frac{L_{t2}}{D_{tu}} \rho_f \frac{V_{mt}^2}{2} + 0.42 \rho_f \frac{V_{mt}^2}{2} \tag{18}$$

$$+ (1 - \frac{A_t^2}{A_{hs}^2}) \rho_f \frac{V_{mt}^2}{2} + 0.42 (1 - \frac{A_t^2}{A_{hs}^2}) \rho_f \frac{V_{mt}^2}{2} + \rho_f \frac{V_{mt}^2}{2} \tag{20}$$

Finally the pumping power can be evaluated through the following equation,

$$Pp = \Delta p_{tot} \times G \tag{19}$$

The friction factor that appears in the total pressure drop equation is evaluated using the correlation provided by Copeland [12],

$$f\,\mathrm{Re} = [(3.2(\frac{\mathrm{Re} D_h}{L})^{0.52})^2 + (4.7 + 19.64B)^2]^{0.5} \tag{20}$$

where *B* is a geometrical parameter given by ,

$$B = \frac{(\frac{1}{\alpha})^2 + 1}{(\frac{1}{\alpha} + 1)^2} \tag{21}$$

3. Optimization procedure

In this paper, two design variables are selected; the channel aspect ratio (α) and the fin spacing ratio (β). The limits of these design variables are taken from Kleiner et al. [10] with $23.742 < \alpha < 59.808$ and $0.254 < \beta < 0.5$. The system is treated as a multi-objective function with the thermal resistance (Eqn. 15) and the pumping power (Eqn. 19) being the first and the second objectives. These objective functions are optimized using the NSGA-II.

3.1. The applied algorithm

The objective functions considered in the current study posses a competing nature in which the increase in one results in a decrease in the other. The NSGA-II known for its strong capability in optimizing multi-objective functions [13], is used to perform the optimization process. The methodology applied to perform the optimization and hence to generate the Pareto optimal front is fully described in Ahmed et al. [14].

4. Results and discussion

In this section, the overall performance of the considered system is investigated for four different coolants, air, ammonia gas, R-12 and R-22. For a constant volumetric flow rate (G = 5.3 l/s) and under the same operating conditions (Table 1), the performance of the system with air as a coolant is used as a benchmark for comparison with other coolant performances as it can be seen in Figs. 2 and 3 for ammonia gas, and R-12 and R-22, respectively.

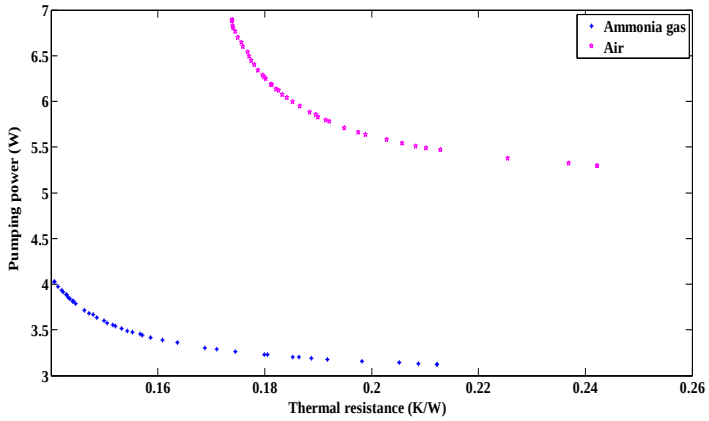

Fig. 2. The overall performance of the considered system with air vs. ammonia gas.

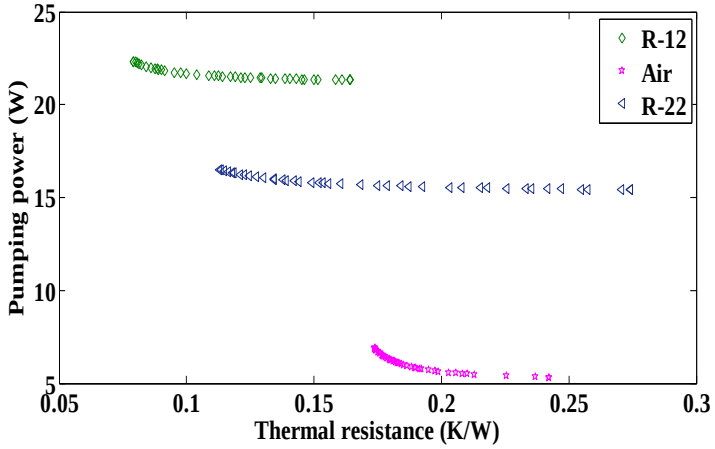

Fig. 3. The overall performance of the considered system with air vs. R-12 and R-22.

It can clearly be seen from Fig. 2 that ammonia gas behaves better than air as a cooling fluid. It provided a significant reduction in the total thermal resistance and pumping power for the same operating conditions. This behavior is attributed to the excellent thermophysical properties of ammonia. The specific heat capacity and the thermal conductivity of ammonia are better than air in the expected range of operating temperature. As for air vs. R-12 and R-22 (Fig. 3), the latter two provided much lower thermal resistance than air but at the expense of the required pumping power. The Montreal Protocol has stopped any industrial application of R-12 due to its significant contributions to the Global Warming Phenomena (GWP) and Ozone Depleting Potential (ODP).

Table 1 Assumed parameters and thermophysical properties at 27 oC.

Parameters	Values
Heat sink lateral dimensions, (W×L) (cm^2)	5×5
Channel height, H_c (cm)	2.5
Induction tubes length, L_t (m)	0.5
Induction tubes diameter, D_t (mm)	19
Thermal conductivity of aluminum, k_w(W/m.K)	238

R-22 lowers the thermal resistance significantly compared to air but with a very high pumping power requirement too. It can be seen that ammonia gas showed a reasonable performance in both aspects, thermal and hydrodynamic, compared to the other coolants considered in this research. Known for its environmental friendly behavior and not requiring sophisticated machinery to be produced, ammonia gas can be a very suitable alternative for air and water generally used in the heat sinks. The optimized results of the current study are listed in Table 2.

Table 2. Optimized results of the current study.

Parameters	Air	Ammonia gas	R-12	R-22
Thermal resistance, R (K/W)	0.178	0.14	0.08	0.113
Pumping power, Pp (W)	6.4	4	22.4	16.5
Channel aspect ratio, α	51.799	59.692	58.912	59.785
Fin spacing ratio, β	0.272	0.267	0.254	0.254

5. Conclusions

In this research, the overall performance of a rectangular microchannel heat sink is examined for four different coolants, air, ammonia gas, R-12 and R-22. Ammonia gas showed balance thermal and hydrodynamic performances under the same operating conditions compared to the other coolants investigated in this study. R-12 and R-22 provided a lower thermal resistance but they cannot be considered due to the high pumping power demands and their environmental issues. The results obtained provide motivation for further efforts to be spent on exploration of other coolant performances in the area of microchannel heat sinks industry.

Acknowledgements

The authors would like to acknowledge the supports from Universiti Teknologi Malaysia (UTM) under UTM Razak School Grant Vote No. 4B026 for providing the fund and facilities throughout the course of this research.

References

[1] Garimella, S.V., Singhal, V., 2004. Single-Phase Flow and Heat Transport and Pumping Considerations in Microchannel Heat Sinks, Heat Transfer Engineering 25, p.15.

[2] Garimella, S.V., Singhal, V., Liu, D., 2006. On-Chip Thermal Management with Microchannel Heat Sinks and Integrated Micropumps, Proceeding of IEEE 94, pp.1534-1548.
[3] Goldberg, N., 1984. Narrow Channel Forced Air Heat Sink, IEEE Transaction of Component, Hybrid and Manufacturing Technologies, pp.154-159.
[4] Mohammed, H.A., Bhaskaran, G., Shuaib, N.H., Saidur, R., 2011. Heat Transfer and Fluid Flow Characteristics in Microchannels Heat Exchanger Using Nanofluids: a Review, Renewable and Sustainable Energy Reviews 15, p.1502.
[5] Knight, R.W., Goodling, J.S,, Gross, B.E., 1992. Optimal Thermal Design of Air Cooled Forced Convection Finned Heat Sinks- Experimental Verification, Proceeding of IEEE, pp.206-212.
[6] Aranyosi, A., Bolle, L., Buyse, H., 1997. Compact Air-Cooled Heat Sinks for Power Packages, Proceeding of IEEE, pp.165-177.
[7] Khan, W.A., Yovanovich, M.M., Culhum, J.R., 2009. Optimization of Microchannel Heat Sinks Using Entropy Generation Minimization Method, IEEE Transaction on Component and Packages Technologies 32, pp.243-251.
[8] Hu, G., Xu, S., 2009. Optimization Design of Microchannel Heat Sink Based on SQP Method and Numerical Simulation, Proceeding of IEEE, pp.89-92.
[9] Wen, Z., Choo, F., 1997. Optimum Thermal Design of Microchannel Heat Sinks, Proceeding of IEEE, pp.123-129.
[10] Kleiner, M.B., Kuhn, S.A., Haberger, K., High Performance Forced Air Cooling Scheme Employing Microchannel Heat Exchangers, IEEE Transaction on Component, Packages and Manufacturing Technologies 20, pp.795-804.
[11] Kim, S.J., Kim, D., 1999. Forced Convection in Microstructures for Electronic Equipment Cooling, Journal of Heat Transfer121, p. 639.
[12] Copeland, D., 2000. Optimization of Parallel Plate Heat Sinks for Forced Convection, Proceeding of IEEE, pp.266-272.
[13] Deb, K., Agrawal, S., Partap, A., Meyarivan, T., 2002. A Fast and Elitist Multi-Objective Genetic Algorithm for Multi-Objective Optimization: NSGA-II, Proceeding of the Parallel Problem Solving from Nature VI Conference, Paris, April, pp.849-858.
[14] Ahmed, M.A., Normah, M.G., Robiah, A., 2012. Optimization of an Ammonia-Cooled Rectangular Microchannel Heat Sink Using Multi-Objective Non-Dominated Sorting Genetic Algorithm (NSGA2), Heat and Mass transfer, p.15, doi:10.1007/s00231-012-1016-8.

Available online at www.sciencedirect.com

SciVerse ScienceDirect

Procedia Engineering 00 (2012) 000–000

Procedia Engineering

www.elsevier.com/locate/procedia

5th BSME International Conference on Thermal Engineering

Experimental Investigation of Rheological Behavior and Pressure drop of Aqueous Suspensions of Carbon Nanotubes in a Horizontal Tube

Salma Halelfadl [a*], Thierry Maré [a], Patrice Estellé [b], Normah Mohd-Ghazali[c*]

[a] Laboratoire de Génie Civil et de Génie Mécanique (LGCGM), INSA de Rennes, IUT Saint Malo, France
[b] LGCGM, INSA de Rennes/IUT Rennes, France
[c]Faculty of Mechanical Engineering, UTM, Johor Bahru, Malaysia

Abstract

A new engineering medium, called nanofluid, have attracted a wide range of researches on many processes in engineering applications. Many experimental and theoretical studies on viscosity of nanofluids are controversial and the shear rate dependent viscosity is frequently neglected. The aim of the present work is to investigate the effect of the rheological behavior of aqueous suspensions of carbon nanotubes on the friction factor and the pressure drop in a horizontal tube under laminar and turbulent flow. The particles weight concentration used here is 0.01%. The rheological behavior was measured for a range of temperature from 0°C to 40°C. The results showed that the nanofluids exhibit a shear thinning behavior at very low shear stress. The analysis results of the flow characteristics showed a non-Newtonian behavior under laminar flow and a Newtonian behavior under turbulent flow.

Keywords: *Keywords: Nanofluid, viscosity, shear-thinning, friction factor, pressure drop*

Nomenclature

f	friction coefficient
D	diameter of horizontal tube (m)
g	gravitational constant (m/s²)
Re	Reynolds number
Q	flow rate (m^3/s)
L	length of horizontal tube (m)
Greek symbols	
μ	dynamic viscosity (Pa.s)
ε	roughness (mm)
φ	concentration (%)
ρ	density (kg/m^3)
ΔP	pressure drops (Pa)
Subscripts	
m	weight
nf	nanofluid
0	water
s	surfactant

1. Introduction

Due to the global concern on energy conservation, the development and improvement of heat exchangers in many sectors (automobile, construction, electronics…) have today become a major issue in the industrial world. Therefore, the development of more efficient heat transfer fluids with higher thermal properties is considered urgent. Over the past decade, many researchers have investigated a new kind of heat transfer fluid called nanofluids to improve the heat transfer properties of liquids.

Nanofluids are fluid suspensions of nanometer-sized particles of metals, oxides, carbides, nitrides or nanotubes. They have attracted much attention because of their high thermal conductivity and thermal performances compared to base fluids [1-3]. Many researches have mostly focused on the thermal conductivity of these fluids [4-5]. However, the viscosity also deserves the same attention as thermal conductivity. In fact, viscosity describes the internal resistance of a fluid to flow and is an important property for all thermal applications involving fluids. In addition, the pumping power is related to the viscosity of a fluid. The addition of solid nanoparticles to a base fluid may lead to an increased viscosity and a significant pressure drop which can reduce the practical benefits of nanofluids in some industrial applications [6]. Numerous experimental and theoretical investigations have been carried out on viscosity and rheological behavior of nanofluids [7-12]. All these studies reported that viscosity of nanofluids increased with an increase of nanoparticles concentration and decreased with an increase of temperature. Compared to the thermal performances, the hydrodynamic behavior of nanofluids, especially for carbon nanotubes based nanofluids, has been rarely reported. In this present work, the focus is on an aqueous multi-walled carbon nanotubes based nanofluid at low weight concentration (0.01%). The effect of the viscosity and the hydrodynamics characteristics at ambient temperature is investigated in order to compare the experimental results on fraction factor between the nanofluid and pure water in a horizontal tube. Finally, the experimental data are analyzed using traditional equations for friction factor to evaluate the effect of the rheological behavior on nanofluid flow under laminar and turbulent conditions.

2. Experimental and data analysis

2.1. Nanofluids

An aqueous carbon nanotubes based nanofluid was provided by Nanocyl™ (Belgium). This suspension consists of thin multi-walled carbon nanotubes (carbon purity 90%) dispersed in a mixture of de-ionized water and surfactant from ultra-sonication (fig. 1). The characteristics of the basic solution are summarized in Table1. De-ionized water was used to dilute the basic solution (1% wt) and prepare the suspension of 0.01% in mass concentration. The mixture is stirred with a mixer for 30min then left at rest and the process was repeated 24 hours later. The purpose of the mechanical stirring is to ensure a uniform dispersion of nanoparticles and prevent initial agglomerating of nanoparticles in the base fluid.

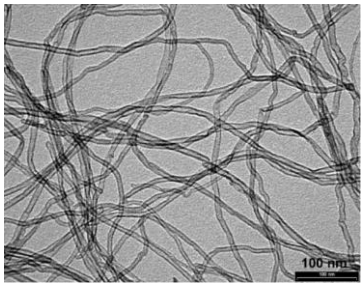

Figure 1: Tunneling Electron Microscopy (TEM) images of synthesized MWNTs by Nanocyl ™

Table I: Characteristics of CNT basic solution (1%wt)

Supplier	Nanoparticles	Size	φ_m(nf)	dispersant
Nanocyl	Multi-Walled Carbon nanotubes	D : 9-10nm L : 1.5µm	1%	SDBS φ_m(s)=2%

2.2. Rheological behavior

The rheological measurements of nanofluid are performed using a stress controlled rheometer Malvern Kinexus Pro equipped with a cone and plate geometry. . The cone diameter is 60mm and the cone angle is 1°. This leads to a measurement gap of 0.03mm. The temperature was controlled using a Peltier temperature control device located below the lower plate with an accuracy of 0.01 ° C. The temperature is maintained constant 5 min before starting the test, which allows for the sample's constant temperature condition and complies with standards. The experimental procedure involves applying a logarithmic stress ramp under steady-state conditions with maximum step duration of 180s. When a steady-state flow condition is achieved and maintained 10s, the shear rate is measured. The range of shear stress applied was between 0.01 and 0.5 Pa which ensures a steady flow for low shear rate and stability of the flow at high shear rate. During each test, the viscosity was measured as a function of temperature from 0 to 40°C. The tests were repeated to verify the reproducibility of the measurement and the suspensions stability with time.

Distilled water and standard oil were tested as calibration fluids at 20 ° C to validate the experimental protocol used in this study. The results showed a Newtonian behavior for these fluids. Moreover, the dynamic viscosity measured at 20 °C is 1.03mPa.s for water and 1360mPa.s for oil, which represents a relative error less than 3% (water) and 4% (standard oil) in comparison with the theoretical values. These results validated the experimental protocol.

2.3. Experimental protocol: Hydrodynamic

A sketch of the horizontal flow that was used during the present study is illustrated in figure 2. A centrifugal pump (2) was sucking water from a reservoir (1) and the flow rate was controlled with a valve (3). The test section consists of a cylindrical PVC tube (5) of 333mm length, 19mm in inner diameter and 0.0015mm in roughness. Static pressure taps, at the test section are connected to piezometric tubes to assess the losses. The experimental setup contains a diaphragm for measuring the flow of water. The flow of nanofluid is obtained directly by measuring the time to fill a container of a known volume. The tests were performed on distillated water in laminar and turbulent flow conditions in order to validate the experimental protocol.

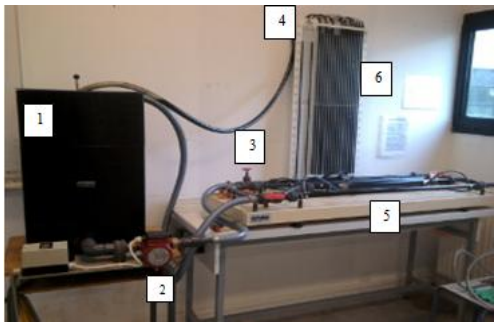

Figure 2: Experimental set up

The friction coefficient is calculated from the two following models. Experimental model (see equation 1) is related to experimental results of linear pressure drops in the tube. Whereas, theoretical model is linked to classical equation for friction coefficient under laminar (equation 2) and turbulent flow (equation 3).

$$f = \left(\frac{D}{L}\right)\frac{\Delta P}{\rho u^2/2} \tag{1}$$

$$f = \frac{64}{\mathrm{Re}} \quad Or \quad f = \mu\frac{16\pi D}{\rho}Q \tag{2}$$

$$\frac{1}{\sqrt{f}} = -2\log_{10}\left(\frac{2.51}{\mathrm{Re}\sqrt{f}} + \frac{\varepsilon}{3.71D}\right) \tag{3}$$

The density measurements were performed on Anton PAAR DMA vibrating tube densimeter connected to cell 602 with a high precision of 1.10-5 g/cm3.The density of the nanofluid measured at 20 ° C is 999, 603 kg/m^3.

Preliminary Measurements were performed on pure water in order to validate the experimental protocol. Figure 3 shows the evolution of the friction factor for experimental and theoretical data as a function of Reynolds number. The results show that the theoretical models (Eq. 2; 3) are in accordance with experimental measurements with a relative error of 5%. These results allowed the validation of the experimental protocol.

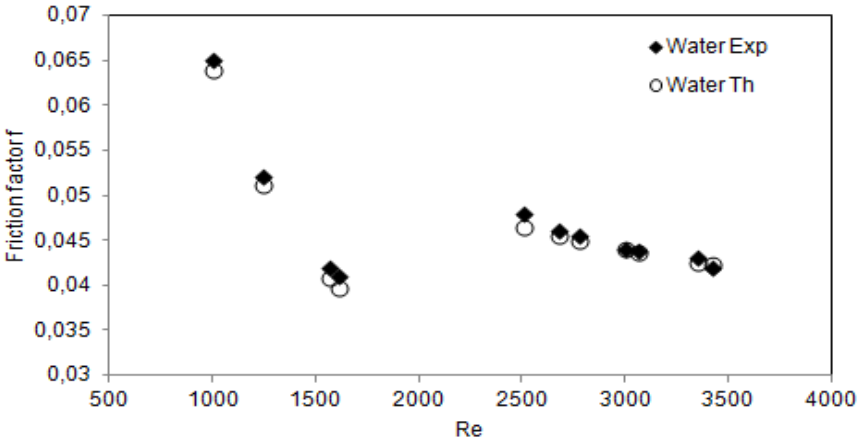

Figure 3: Experimental and theoretical friction factor of distillated water

3. Results

3.1. Rheological behavior

Figure 4 shows the evolution of the apparent dynamic viscosity as a function of shear rate for a range of temperature from 0 to 40°C. The results showed that the nanofluid viscosity decreases with an increase of temperature. For low shear rate (less than 100s^{-1}), the nanofluid behaves like a shear thinning fluid, as the apparent viscosity decreases with the increase of shear rate. For higher shear rates, the viscosity is independent of the applied shear rate and the nanofluid is Newtonian.

In the next section, we focus on the rheological behavior of nanofluid at low shear rates (0-200 s^{-1}) at 20 ° C because the hydrodynamic study was carried out at room temperature (20 ° C). Based on the results of Figure 8, the nanofluid is non Newtonian for very low shear rate (less than 80-100s^{-1}). The dynamic viscosity measured at high shear rate is μ_{nf} = 0.99915 mPa.s (very close to that of pure water). However, we can note that nanofluid at 0.01 weight concentration have lower shear viscosity than water due to the lubricative effect of nanoparticles [14].

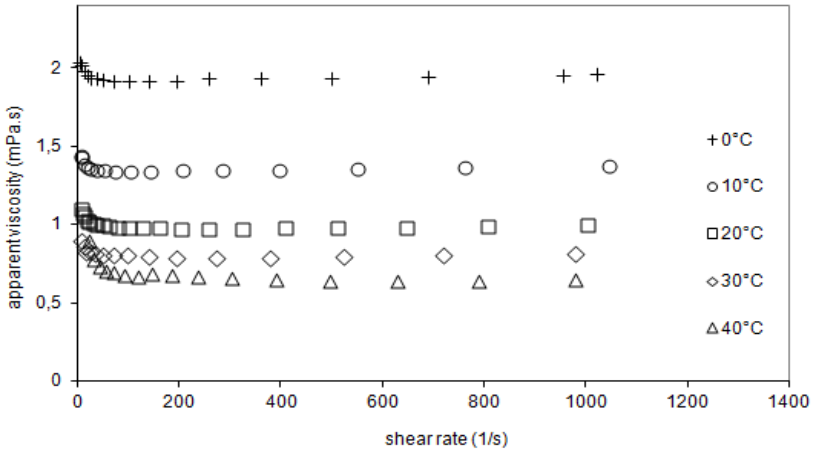

Figure 4: Viscosity as a function of shear rate for different temperatures

3.2. Hydrodynamic behavior

Figure 5 shows the evolution of pressure drop as a function of volumetric flow rate. We can observe that the nanofluid behave similarly as pure water with a slightly higher pressure drop. The results showed two different zones, low flow rates (less than 0,025 l/s) and high flow rates (greater than 0.038l/s) where the pressure drops become much more important. These zones correspond respectively to laminar and turbulent flow. It is observed from figure 5 that at low flow rates, the pressure drops of the nanofluid are larger than the ones of distilled water. As the flow rate increases, the pressure drops of both nanofluids and the distilled water become almost the same.

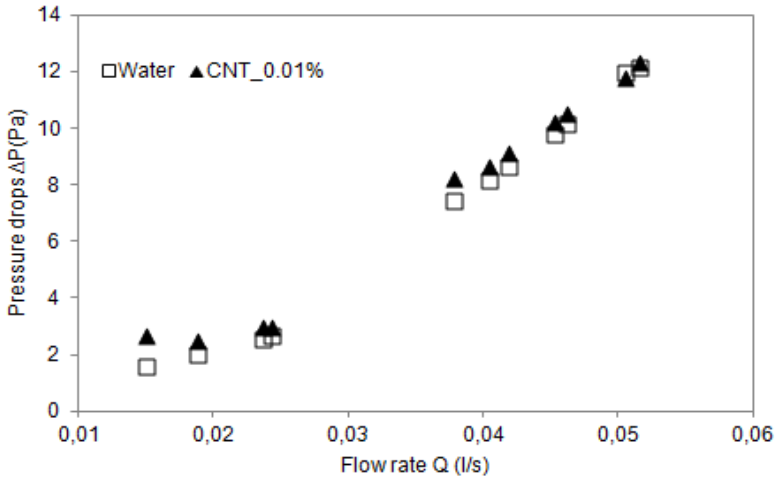

Figure 5: Linear pressure drops of CNT/water and distillate water

Figure 6 reports the evolution of the experimental and theoretical friction coefficient of the nanofluid with the flow rate. The experimental friction coefficient was obtained based on the results of Figure 4 and using equation 1. The theoretical coefficient is obtained by assuming that the nanofluid behave as a Newtonian fluid (Eq. 2 and Eq. 3) and applying the value of the viscosity measured previously (μnf= 0.000956 Pa.s). At low flow rate, the experimental results are different from the theoretical model. This is because, as seen in figure 4, the rheological behaviour of the nanofluid is non-Newtonian at very low shear rate. As the flow rate increases, contrary to this, the difference between the experimental and the theoretical results become very small and the nanofluid behaves as a Newtonian fluid. This shows that the Newtonian model is not valid for low flow rate and that the viscosity is dependent on the applied flow (at low shear rate).

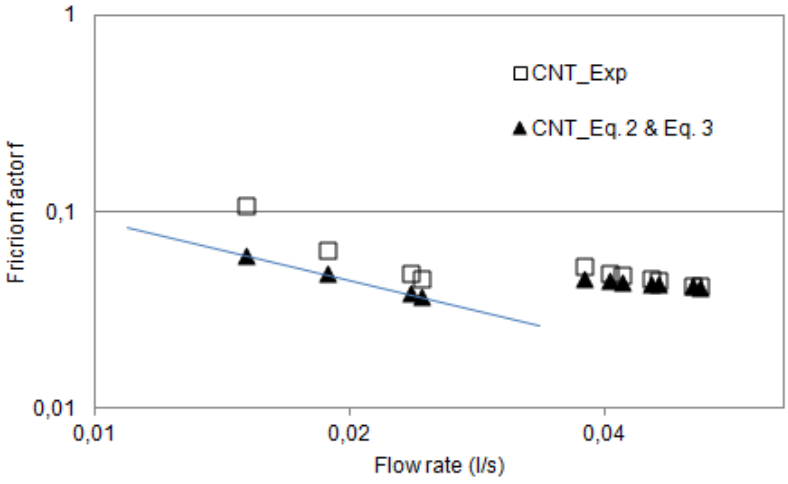

Figure 6: Experimental and theoretical friction factor of CNT/water

4. Conclusion

In this work, we studied the rheological behaviour of a nanofluid based on carbon nanotubes dispersed in water with a weight concentration of 0.01% as a function of temperature and shear rate. The nanofluid behaves as a Newtonian for high shear rates (greater than 100s-1). At a low shear rate, the nanofluid is non-Newtonian. We also studied the hydrodynamic behaviour of the nanofluid in a horizontal cylindrical pipe. The results have shown that the evolution of the experimental friction factor does not follow the classical model of Newtonian fluids for low flow rate. This can be explained by the rheological behaviour of nanofluid at very low and at high shear rates.

Section headings should be left justified, with the first letter capitalized and numbered consecutively, starting with the Introduction. Sub-section headings should be in capital and lower-case italic letters, numbered 1.1, 1.2, etc, and left justified, with second and subsequent lines indented. You may need to insert a page break to keep a heading with its text.

Acknowledgements

Nanocycl Belgium is gratefully acknowledged for providing the CNT water based nanofluid.

References

[1] Maré T., , Halelfadl S., Sow O., Estellé P., Duret S., Bazantay F., Comparison of the thermal performances of two nanofluids at low temperature in a plate heat exchanger, Experimental Thermal and Fluid Science, 35/8, 1535-1543, 2011

[2] Wen D.S., Ding Y.L., Effective thermal conductivity of aqueous suspensions of carbon nanotubes (nanofluids), J. Thermophys. Heat Transfer, Vol.18 4, pp. 481-485, 2004.

[3] Wang XQ, Mujumdar AS, Heat transfer characteristics of nanofluids: A review, Int. J. Therm. Sci., Vol. 46/1, pp. 1-19, 2007.

[4] Choi, S., 'Enhancing thermal conductivity of fluids with nanoparticules', In Developments Applications of Non -Newtonians Flows, D.A. Siginer and H. P. Wang. New-York : Americain society of Mechanical Engineers, Vol. 66, pp. 99-105, 1995.

[5] Murshed SMS Leong KC, Yang C, Investigations of thermal conductivity and viscosity of nanofluids, Int. J. Therm. Sci., Vol. 47 pp. 560-568, 2008.

[6] Ferrouillat S., Bontemps A., Ribeiro J. P., Gruss J. A., Soriano O., Hydraulic and heat transfer study of SiO_2/Water nanofluids in horizontal tubes with imposed wall temperature boundary conditions, Int. Journal of Heat and Fluid Flow, Vol. 32, pp. 424-439, 2011.

[7] Nguyen C.T., Desgranges F., Roy G., Galanis N., Maré T., Butcher S. , Angue Mintsa H., Temperature and particle-size depends viscosity dated heart water-based nanofluids - Hysteresis phenomenon, International Journal of Heat of and Fluid Flow, Vol. 28, Exit 6, pp. 1492-1506, 2007.

[8] Aladag B., Halelfadl S., Doner N., Maré T., Duret S., Estellé P., Experimental investigations of the viscosity of nanofluids at low temperatures, Applied Energy, Vol. 97, pp. 876-880, 2012.

[9] Phuoc T. X., Massoudi M., Chen R. H., Viscosity and thermal conductivity of nanofluids containing carbon nanotubes stabilized by chitosan, Int J. Thermal Sci., Vol. 50, pp. 12-18, 2011.

[10] Nguyen C.T., Desgranges F., Roy G., Galanis N., Maré T., Butcher S., Angue Mintsa H., Viscosity data for Al2O3 water nanofluid hysteresis: is heat transfer enhancement using nanofluids reliable?, International Journal of Thermal Sciences, Vol. 47, pp. 103-111, 2008.

[11] Chen H., Ding Y., Lapkin A., Rheological behavior of nanofluids containing tube/rod-like nanoparticles, Power Technology, vol. 194, pp. 132-141, 2009.

[12] Lee W. S., Dae S. P., Kang S., Bang I. C., Kim J. H., investigation of viscosity and thermal conductivity of SiC nanofluids for heat transfer applications, International Journal of Heat and Mass Transfer, vol. 54, pp. 433-438, 2011.

[13] Chen L. , Xie H., Yu W., Li Y., The rheological behaviors of nanofluids containing multi-walled carbon nanotube, Journal of Dispersion Science and Technology, vol. 32/4, 2011.

[14] Chen L., Xie H., Yu W., Li Y., The rheological behaviors of nanofluids containing multi-walled carbon nanotube, Journal of Dispersion Science and Technology, Vol. 32/4, 2011.

Available online at www.sciencedirect.com

SciVerse ScienceDirect

Procedia Engineering 00 (2012) 000–000

Procedia Engineering

www.elsevier.com/locate/procedia

5th BSME International Conference on Thermal Engineering

Natural convection of nanofluids in open rectangular cavity

M. Saleem[a,*] , M. A. Hossain[b], S. C. Saha[c]

[a]*COMSATS Intitute of Information Technology, Chak Shahzad, Islamabd, Pakistan*
[b]*Rtd. Professor, University of Dhaka, Dhaka, Bangladesh*
[c]*School of Engineering Systems, Queensland University of Technology Brisbane, Australia*

Abstract

An investigation of the effect of nano particles on natural convection of water based nanofluids contained in an open rectangular cavity is carried out numerically. The flow pattern and heat transfer characteristics are studied for different values of volume fraction in the range $0 \le \phi \le 0.2$, Rayleigh number in the range $1 \le Ra \le 10^9$ and the nano particles with different thermo physical properties. It was found that for low Rayleigh numbers, heat transfer exhibits a decreasing trend for increasing values of volume fraction of oxide nanofluids, whereas for higher values of Rayleigh numbers, an increasing trend of heat transfer was observed due to increase in the volume fraction of nanofluids.

Keywords: Natural convection; Nano Fluids; Open Cavity.

Nomenclature

A	aspect ratio	x, y	non dimensional coordinate axis
C_p	specific heat at constant pressure (JK^{-1})	*Greek symbols*	
g	acceleration due to gravity (ms^{-2})	α	thermal diffusivity $(k/\rho C_p)$
H	height of the enclosure	β	thermal expansion coefficient (K^{-1})
h	mesh spacing	θ	non dimensional temperature
(i, j)	nodal locations of (x, y) on grid	μ	dynamic viscosity $(m^{-1}s^{-1})$
I, J	maximum grids along coordinate axis	ν	kinematic viscosity $m^2s^{-1}Kg^{-1}$
k	thermal conductivity $(Wm^{-1}K^{-1})$	ρ	density of fluid (Kgm^{-3})
L	length of the cavity	ϕ	nano particles volume fraction
Nu	local Nusselt number	$\overline{\psi}$	stream function $(m^2s^{-1}Kg^{-1})$
$\overline{Nu}$	average Nusselt number	ψ	non dimensional stream function
$\overline{p}$	fluid pressure (Pa)	$\overline{\omega}$	dimensional vorticity function (s^{-1})
Pr	Prandtl number of fluid	ω	non dimensional vorticity function
Ra	Raleigh number	*Subscripts*	
$\overline{T}$	dimensional temperature (K)	s	solid particles properties
$\overline{T}_H, \overline{T}_C$	maximum and minimum temperature (K)	f	fluid properties
$\overline{T}_0$	average/reference temperature (K)	nf	nanofluid properties
$\bar{t}$	dimensional time (s)	eff	effective property
t	non dimensional time	in	incoming

$\bar{u},\bar{v}$	velocity components (ms^{-1})	*out*	outgoing
u,v	non dimensional velocity components	0	reference state
$\bar{x},\bar{y}$	dimensional coordinate axis (m)		

1. Introduction

Nano fluid is a remarkable advancement in heat transfer engineering, as it has numerous applications in the practical situations where enhanced heat transfer is required. Heat transfer enhancement can be acheived by suspending nano size solid particles of relatively larger thermal conductivity in pure fluids. This idea of nanofluids was first proposed by Choi [1]. Khanafer et al. [2] numerically investigated the natural convection of nanofluids in a two dimensional enclosure. They considered different models of nanofluids and showed that the heat transfer of nanofluids is greater than that of pure fluid for all values of Grashof number. Hwang et al. [3] conducted the buoyancy-driven heat transfer study of water-based Al_2O_3 nanofluids in a rectangular cavity. Ho et al. [4] considered natural convection of nanofluid in a square enclosure. They used water $-Al_2O_3$ nano fluid to compare the heat transfer for four different models of effective dynamic viscosity and effective thermal conductivity that were found in literature. Oztop and Abu-Nada [5] considered natural convection of water based nanofluids in partially heated rectangular enclosures. They considered three different types of nano particles namely Copper (Cu), Al_2O_3 and TiO_3. They considered the volume fraction in the range $0 \le \phi \le 0.2$. The implementation of boundary conditions for open ended rectangular domains differ a lot from the usual solid wall boundary conditions. A detailed description can be seen in Roache[6], whereas recent work on open ended domains is considered by Saleem et al. [7,8]. We consider the natural convection of water based nanofluid in an open rectangular domain, and focus on investigating the heat transfer of nanofluids in open ended domain.

2. Mathematical Formulation

Consider two-dimensional flow of a nanofluid confined in an open rectangular cavity of length L and height H. The left wall is assumed to be at temperature $\bar{T}_H$. The temperature of the fluid that enters the cavity region from the right end is supposed $\bar{T}_C$ at $\bar{t} = 0$ (where $\bar{T}_H > \bar{T}_C$). We use the subscripts 'in' for incoming, and 'out' for outgoing fluid respectively. Moreover the subscripts 's' and 'f' are respectively taken for physical properties of solid particles and pure fluid, whereas the subscript 'nf' stands for the physical properties of nanofluid. Flow configuration and physical boundary conditions are shown in Figure 1.

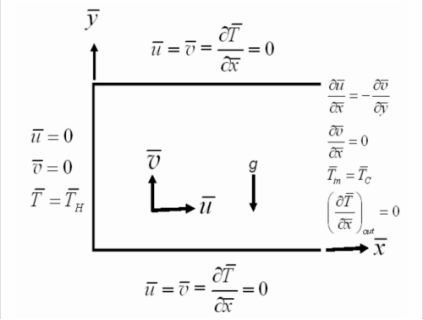

Fig.1. Flow configuration in coordinate system

Let ϕ be the volume fraction of nanoparticles with in the fluid, and ρ_s, ρ_f be the densities of the solid particles and the fluid respectively, then the effective density of the nanofluid is given by (see Khanafer et al. [2], Oztop and Abu-Nada [5])

$$\rho_{nf} = (1-\phi)\phi_f + \phi\rho_s \tag{1}$$

Like wise the effective heat capacity for nanofluid is expressed as

$$(\rho C_p)_{nf} = (1-\phi)(\rho C_p)_f + \phi(\rho C_p)_s \tag{2}$$

Further we approximate the effective thermal conductivity of the nanofluid by the relation

$$k_{eff} = \frac{k_{nf}}{k_f} = \frac{k_s + 2k_f - 2\phi(k_f - k_s)}{k_s + 2k_f + \phi(k_f - k_s)} \tag{3}$$

Moreover the viscosity of nanofluid is given by

$$\mu_{nf} = \frac{\mu_f}{(1-\phi)^{2.5}} \tag{4}$$

Here the effective thermal conductivity and the effective dynamic viscosity are chosen in view of the maximum heat transfer enhancement (see also [3-5]). Finally the thermal diffusivity of nanofluid is given by

$$\alpha_{nf} = \frac{k_{nf}}{(\rho C_p)_{nf}} \tag{5}$$

Further we introduce the non dimensional variables by using the following transformations for stream vorticity form

$$\begin{gathered} x = \frac{\bar{x}}{H}, \quad y = \frac{\bar{y}}{H}, \quad t = \bar{t}\,\frac{\alpha_f}{H^2}, \quad u = \bar{u}\,\frac{H}{\alpha_f}, \quad v = \bar{v}\,\frac{H}{\alpha_f}, \\ \psi = \frac{\bar{\psi}}{\alpha_f}, \quad \omega = \bar{\omega}\,\frac{H^2}{\alpha_f}, \qquad \theta = \frac{\bar{T} - \bar{T}_C}{T_H - \bar{T}_C}, \quad A = \frac{L}{H} \end{gathered} \tag{6}$$

where x, y are the non dimensional coordinate axis, u, v are the non dimensional velocity components, ψ and ω are the non dimensional stream and vorticity functions, t is the non dimensional time, θ is the non dimensional temperature, whereas A is the aspect ratio of the cavity. By making use of these dimensionless parameters, for the unsteady motion of nanofluid, the Navier Stokes equations in stream-vorticity form, along with the energy equation in dimensionless rectangular coordinate system are given by (see [3-5])

$$\frac{\partial^2 \psi}{\partial x^2} + \frac{\partial^2 \psi}{\partial y^2} = -\omega \tag{7}$$

$$\frac{\partial \omega}{\partial t} + u\frac{\partial \omega}{\partial x} + v\frac{\partial \omega}{\partial y} = \left[\frac{\Pr}{(1-\phi)^{0.25}\left\{(1-\phi) + \phi\frac{\rho_s}{\phi_f}\right\}}\right]\left(\frac{\partial^2 \omega}{\partial x^2} + \frac{\partial^2 \omega}{\partial y^2}\right) + Ra\,\Pr\left[\frac{1}{\frac{(1-\phi)}{\phi}\frac{\rho_f}{\rho_s} + 1}\frac{\beta_s}{\beta_f} + \frac{1}{\frac{\phi}{(1-\phi)}\frac{\rho_f}{\rho_s} + 1}\right]\frac{\partial \theta}{\partial x} \tag{8}$$

$$\frac{\partial \theta}{\partial t} + u\frac{\partial \theta}{\partial x} + v\frac{\partial \theta}{\partial y} = \lambda\left(\frac{\partial^2 \theta}{\partial x^2} + \frac{\partial^2 \theta}{\partial y^2}\right) \tag{9}$$

with the following boundary conditions (see [6-8])

$$\begin{gathered} t < 0 \;\; u = v = \psi = \omega = \theta = 0 \quad 0 \le y \le 1 \quad 0 \le x \le A \\ t \ge 0 \;\; u = v = \psi = 0, \quad \omega = -\frac{\partial u}{\partial y}, \quad \frac{\partial \theta}{\partial y} = 0, \quad y = 0 \quad 0 \le x \le A \\ u = v = \psi = 0, \quad \omega = -\frac{\partial u}{\partial y}, \quad \frac{\partial \theta}{\partial y} = 0, \quad y = 1 \quad 0 \le x \le A \\ u = v = \psi = 0, \qquad \omega = \frac{\partial v}{\partial x}, \qquad \theta = 1 \quad x = 0 \quad 0 \le y \le 1 \\ \frac{\partial u}{\partial x} = -\frac{\partial v}{\partial y}, \qquad \omega_{in} = \theta_{in} = 0 \qquad x = A \qquad 0 \le y \le 1 \\ \frac{\partial v}{\partial x} = \left(\frac{\partial \omega}{\partial x}\right)_{out} = \left(\frac{\partial \theta}{\partial x}\right)_{out} = 0 \qquad x = A \qquad 0 \le y \le 1 \end{gathered} \tag{10}$$

where

$$\Pr = \frac{\nu_f}{\alpha_f}, \quad Ra = \frac{g\beta_f (T_H - \bar{T}_C) H^3}{\alpha_f \nu_f}, \quad \lambda = \frac{\frac{k_{nf}}{k_f}}{(1-\phi) + \phi\frac{(\rho C_p)_s}{(\rho C_p)_f}} \tag{11}$$

are respectively the Prandtl number, the Rayleigh number and the diffusion coefficient for the energy equation of nanofluid. We finally define the dimensionless local and average heat transfer rate of the left wall for nanofluid the following relations (see also [5]).

$$Nu = -k_{eff}\left(\frac{\partial \theta}{\partial x}\right)_{x=0} \qquad \bar{N}u = \int_0^1 Nu\,dy \tag{12}$$

where dy is the element of length y along the wall. In order to compare the heat transfer characteristics pure fluid and the fluid with nano-particles, we consider three different water based nanofluid combinations. The physical properties of the fluid and nano-particles are given in table 1. (see[5])

Table 1. Thermo physical properties of pure fluid (water) and nano particles under consideration

Physical properties	Pure fluid Water (H_2O)	Copper Cu	Aluminum Oxide Al_2O_3	Telinium Oxide TiO_3
C_p	4179	385	765	686.2
ρ	997.1	8933	3970	4250
k	0.613	400	40	8.9538
α	1.47×10^{-7}	1.1631×10^{-4}	1.317×10^{-5}	3.07×10^{-6}
β	2.1×10^{6}	1.67×10^{5}	8.5×10^{4}	9×10^{4}

3. Method of Solution

The dimensionless form of the governing equations given by (8) and (9) are descretized using the Alternate Direct Implicit method. For non linear terms of these equations, we used the second upwind difference technique. The elliptic partial differential equation (8), is solved using the Successive Over Relaxation technique with residual tolerance of the order of 10^{-5}. The solution is complemented with the descretized form of boundary conditions given in equations (10). With H as the reference height of the cavity, we have considered a uniform grid of size $h = H/(J-1)$, where J is the maximum number of grids along coordinate axes. Throughout the computation we take $H = 1$. In order to meet the convergence to the steady state, we have considered the tolerance of order 10^{-8}. Further details of the employed method can also be found in [6-8]. All computations are performed for $A = 2$. Intel 1.83 GHz C machine is used for the entire computation.

4. Results and Discussion

We have considered the natural convection of water based nanofluid in an open rectangular cavity. The left wall is considered at a higher temperature than the one of the opening. The effect of volume fraction of nano particles, and Rayleigh number for three different nanofluids is studied. The result are graphically represented in terms of streamlines, isotherms, and heat transfer rate for different values of these governing parameters.

4.1 *The Effect of Volume Fraction*

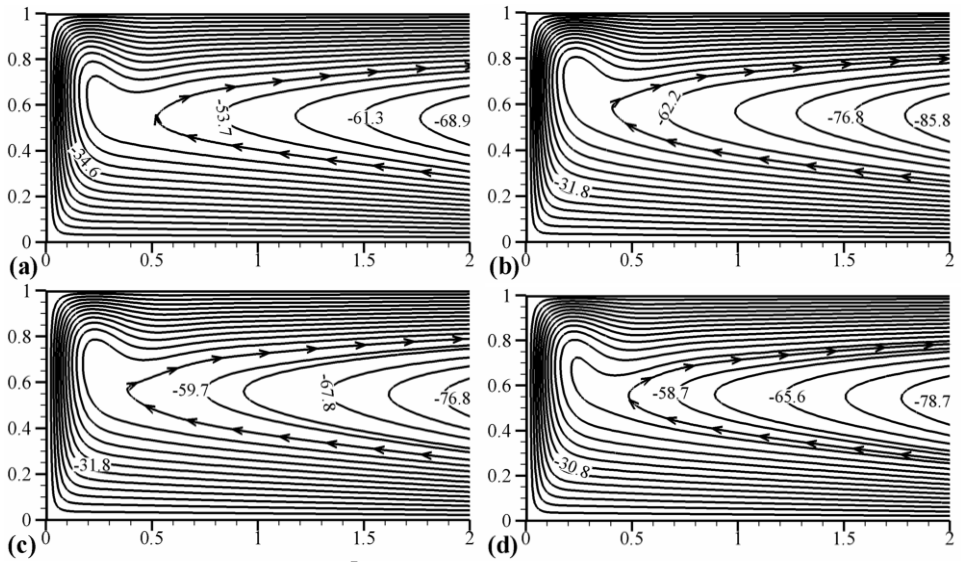

Fig.2. Comparison of streamlines pattern at $Ra = 5\times10^5$, $\Pr = 6.2$, A =2 for (a) pure fluid (water $\beta_s = \phi = 0$), (b) water-copper nanofluid ($\beta_s = 1.67\times10^5, \phi = 0.05$) (c) water- Al_2O_3 nanofluid ($\beta_s = 0.85\times10^5, \phi = 0.05$) (d) water- TiO_3 nanofluid ($\beta_s = 0.9\times10^5, \phi = 0.05$)

Figure 2 represents the comparison of streamlines between pure fluid (water) and water based nanofluids while $Ra = 5\times10^5$, $\Pr = 6.2$. Figure 2 (a) represents the streamline pattern for pure fluid. Comparing Figure 2 (a) and 2 (b), we see that the magnitude of the strength of flow close to the opening in case of water is 68.9, whereas it is 85.8 in case of

water-Cu nanofluid. Thus the flow strength of nanofluid is greater than that of the pure fluid in this case. Figure 2 (c) and 2 (d)show the stream line pattern for water-Al_2O_3 and water-TiO_3 nano fluids, whereas their strength is numerically 76.8 and 78.7 respectively. From Figure 2, it can be discerned that the flow in case of nanofluid increases. Moreover, comparing Figure 2 (b)-2 (d) one can see that the strength of metal based nanofluid is maximum. Although the nanofluids of oxides have greater strength than that of the pure fluid, yet the flow is not more than that of the water-Cu nanofluid.

Let us now consider the effect of volume fraction on these nanofluids separately. Figure 3 shows the average heat transfer rate as a function of volume fraction for (a) water-Cu, (b) water-Al_2O_3 and (c) water-TiO_3 nanofluids while Pr=6.2 at four different values of Rayleigh number. Let us first consider Figure 3 (a). It can be seen that heat transfer increases with the increase in volume fraction of solid particles. Even at $Ra=10^3$, heat transfer increases from 0.775 to 1.3, which does not seem significant due to large scale of the figure along $y-axis$. Now comparing 3 (a) with 3 (b) and 3 (c), we observe that this increasing trend is more prominent in water-Cu nanofluid for $Ra=10^4,10^5,10^6$. For instance at $Ra=10^6$, in Figure 3 (a), heat transfer increases from 22.6 to 38.3 between $0\le\phi\le0.2$ for water-Cu nanofluid, whereas it reaches up to 32.6 for water-Al_2O_3 as in Figure 3 (b), and has a maximum value of 31.6 in case of water-TiO_3 nanofluid at $\phi=0.2$ as shown in Figure 3 (c). However the behavior of heat transfer in Figure 3 (b) and 3 (c) at $Ra=10^3$ require some attention. There is a very slight decline in the heat transfer rate at $Ra=10^3$ in Figure 3 (b) and 3 (c), which is not significantly visible due to scale of the Figure. This deviating behavior for water-Al_2O_3 in Figure 3 (b) is such that the heat transfer very slightly increases from 0.775 to 0.779 between $0\le\phi\le0.05$, and then decreases up to 0.602 in the range $0.05\le\phi\le0.2$. This variation of heat transfer water-Al_2O_3 nanofluid was so slight in comparison to the other values in Figure 3 (b) that it was not visible. Now for water-TiO_3 nanofluid, first the heat transfer rate increases from 0.775 to 0.797 in the range $0\le\phi\le0.07$, then it decreases up to 0.704 between $0.07\le\phi\le0.2$. Thus we can say that for water-Cu (metallic) nanofluid, Heat transfer rate increases with volume fraction for all Rayleigh numbers in the Range $10^3\le Ra\le10^6$. However heat transfer does not monotonically increase with volume fraction at $Ra=10^3$, for Al_2O_3 and water-TiO_3 (oxide) nanofluids at $Ra=10^3$.

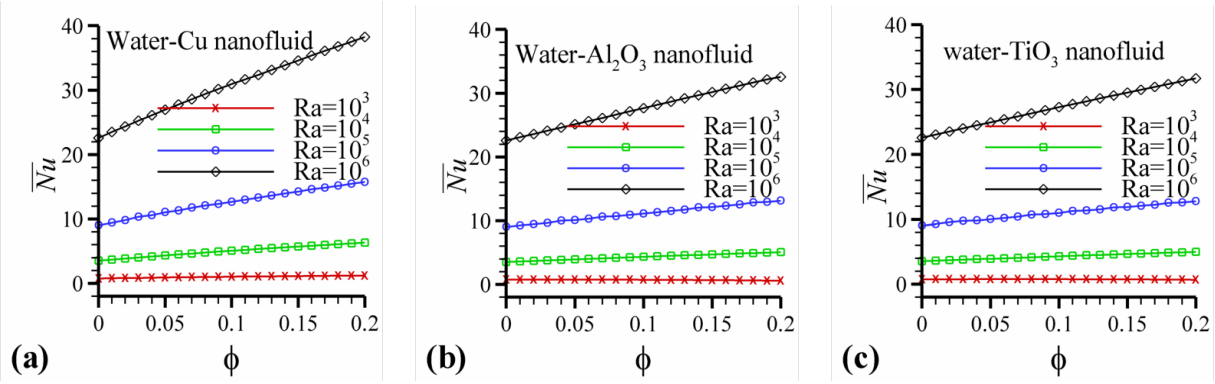

Fig.3. Average heat transfer rates as a function of volume fraction of nanofluids at different values of Rayleigh number for (a) water-Cu nanofluid (b) water-Al_2O_3 nanofluid (c) water-TiO_3 nanofluid combinations

4.2 *The Effect of Rayleigh number*

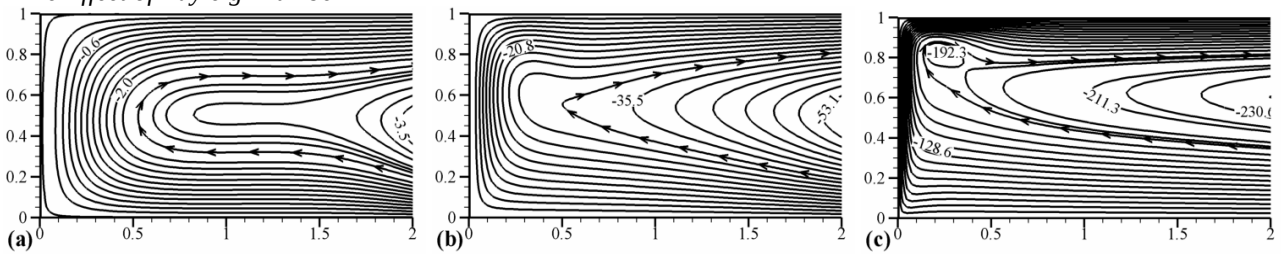

Fig.4. Streamlines of water-TiO_3 nanofluid at $\Pr=6.2$, A=2, $\phi=0.04$, $t=0.5$ for (a) $Ra=10^3$ (b) $Ra=10^5$ (c) $Ra=10^7$

Figure 4 shows the pattern of streamlines of water-TiO_3 nanofluid while $\Pr=6.2$, A=2, $\phi=0.04$, $t=0.5$ for (a) $Ra=10^3$ (b) $Ra=10^5$ (c) $Ra=10^7$ respectively. It can be seen from Figure 4 (a) that at $Ra=10^3$, the strength of flow is very weak. Comparing it with Figure 4 (b) and (c) we see that the strength of the flow increases and the recirculation starts to grow. As can be seen from Figure 4 (c), the strength of flow close to the opening is 230 for $Ra=10^7$, whereas it was

merely 3.5 for $Ra = 10^3$ shown in Figure 4 (a). Finally, Figure 5 shows a comparison of the average heat transfer rate as a function of Rayleigh number for different nanofluids. This Figure also depicts that visible increase in heat transfer for all combinations takes place beyond $Ra > 10^3$. By comparison it can be seen that heat transfer for all nanofluids is greater than the base fluid (water), at any given value of Rayleigh number. However by carefully observing the graph we see that heat transfer in case of water-Cu nanofluid is maximum. For instance at $Ra = 10^8$, Heat transfer rate of pure water is 51.4, whereas its value is 59.0, 58.5, and 57.4 for water-Cu, water-Al_2O_3 nanofluid and water-TiO_3 nanofluid combinations respectively. It can now again be seen that heat transfer of water-Cu nanofluid is maximum among these three at any given value of Rayleigh number.

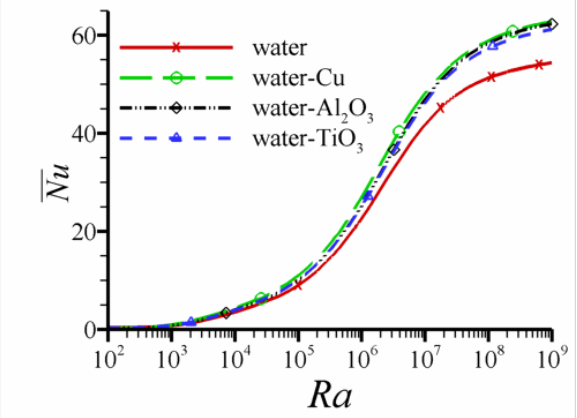

Fig.5. Comparison of the average Nusselt number of heated wall as a function of Rayleigh number, between pure fluid (water $\phi = \beta_s = 0$, $\mathrm{Pr} = 6.2$, A =2), and different water based nanofluid combinations at $\phi = 0.05$, $\mathrm{Pr} = 6.2$, A =2.

5. Conclusions

Natural convection of three different types of water based nanofluids in an open rectangular cavity is numerically studied. It was found that for low Rayleigh numbers ($Ra = 10^3$), heat transfer exhibits a decreasing trend for increasing values of volume fraction of oxide nanofluids in the range $0.05 \le \phi \le 0.2$, whereas for higher values of Rayleigh numbers where the dominant convection takes place ($10^4 \le Ra \le 10^6$, an increasing trend of heat transfer was observed due to increase in the volume fraction of nanofluids. However, water-Cu nanofluid showed an increasing trend for all values of Rayleigh number considered. In comparison to the other two oxide nanofluids considered, water-Cu nano fluid proved to be a better nanofluid in the sense that it has greater heat transfer efficacy and shows an increasing trend for range of Rayleigh number considered. A heat transfer comparison of the nanofluids with that of pure fluid is also made for different values of Raleigh numbers in the range $1 \le Ra \le 10^9$, and it is seen that heat transfer in case of nanofluid is greater than that of the base fluid in the region of dominant convection ($10^3 \le Ra \le 10^9$.

References

[1] S.U.S. Choi, Enhancing thermal conductivity of fluids with nanoparticles, Developments and Applications of Non Newtonian Flows, *FED*-vol. 231/MD-vol. 66, 1995, pp. 99–105.

[2] K. Khanafer, K. Vafai and M. Lightstone, Buoyancy-driven heat transfer enhancement in a two dimensional enclosure utilizing nanofluids, *International Journal of Heat and Mass Transfer*, 2003, vol. 46, pp 3639-3653.

[3] K.S. Hwang, J.H. Lee and S.P. Jang, Buoyancy-driven heat transfer of water-based Al_2O_3 nanofluids in a rectangular cavity, *International Journal of Heat and Mass Transfer*, 2007, vol. 50, pp 4003-4010.

[4] C.J. Ho, M.W. Chen and Z.W. Li, Numerical simulation of natural convection of nanofluid in a square enclosure: Effects due to uncertainties of viscosity and thermal conductivity, *International Journal of Heat and Mass Transfer*, 2008, vol. 51, pp 4506-4516.

[5] Hakan F. Oztop, Eiyad Abu-Nada,Numerical study of natural convection in partially heated rectangular enclosures filled with nanofluids, *International Journal of Heat and Fluid Flow*, 2008, vol. 29, pp 1326-1336.

[6] P.J. Roache, Computational Fluid Dynamics, 2nd edd. Hermosa, Albuquerque, New Mexico, 1998.

[7] M. Saleem, S. Asghar and M.A. Hossain, Natural convection flow in an open rectangular cavity with cold sidewalls and constant volumetric heat source *J. Mechanical Engineering Science Part C*, 2011, vol. 225, pp 1191-1201.

[8] M. Saleem, M.A. Hossain, Shohel Mahmud and Ioan Pop, Entropy generation in Marangoni convection flow of heated fluid in an open ended cavity, *Int. J. Heat and Mass Transfer*, 2011, vol. 54 (3), pp 4473- 4484.

Available online at www.sciencedirect.com

SciVerse ScienceDirect

Procedia Engineering 00 (2012) 000–000

Procedia Engineering

www.elsevier.com/locate/procedia

5th BSME International Conference on Thermal Engineering

Flow behavior and temperature distribution in micro-channels for constant wall heat flux

Md. Jane Alam Khan[a,*], Md. Rakibul Hasan[a,†], Md. Arif Hasan Mamun[a,‡]

[a]*Department of Mechanical Engineering, Bangladesh University of Engineering and Technology (BUET), Dhaka 1000, Bangladesh*

Abstract

An efficient micro-channel heat exchanger was designed which can be used for heat removal from components requiring micro level heat extraction. The heat exchanger is composed of 21 channels and each channel dimensions are 13 x 0.35 x 0.5 mm^3. The channel walls were at no slip and constant heat flux conditions. Different gaseous fluids were considered for the best performance. Hydrogen gave most uniform flow distributions among the channels. The heat exchanger was designed and simulated numerically using the non symmetric pattern multi frontal finite element method for predicting the flow behavior. Five different geometries were proposed and simulated in 2D to find the best geometry in terms of flow distribution. The best geometry was investigated in both 2D and 3D for temperature distributions among the channels. Simulations demonstrated that the effectiveness of the micro-heat exchanger varies with pressure difference, inlet geometry and wall heat flux.

Keywords: CFD; Micro-heat exchanger; Micro-fluid

Nomenclature

C_p	Heat capacity, J/Kg.K
g	Gravitational acceleration, m/s^2
Kn	Knudsen number, Dimensionless
k	Thermal Conductivity, W/m.K
L	Channel Length, µm
M	Mach number
n	Channel number
Re_{max}	Maximum Reynolds number
T_{avg}	Average Temperature, K
T_{max}	Maximum Temperature, K
V_{avg}	Average Velocity, m/s
V_{max}	Maximum Velocity, m/s

* Tel: +88-02-9665636; fax: +88-02-8613046
E-mail address: roninkhan@hotmail.com
† Tel: +88-02-7273246
Email address: rakibhasan_490@hotmail.com
‡ Tel: +88-02-9665636; fax: +88-02-8613046
Email address: mahmamun1@gmail.com

W_a	Channel wall width, µm
W_c	Channel width, µm
Greek symbols	
µ	Dynamic viscosity, Pa.s
ρ	Density, Kg/m^3
Subscripts	
a	wall
c	channel
avg	average value
max	maximum value
min	minimum value

1. Introduction

It is quite obvious that over the past few decades and with the refinement of micro fabrication techniques, the use of micro-channels has become promising for a variety of industrial applications. Micro-channels continue to play an integral part in thermal management (microchip cooling, micro reactors) and energy systems (fuel cells, micro combustion) applications. Moreover, Energy conservation and sustainable development demands have been driving research efforts, within the scope of thermal engineering, towards more energy efficient equipments and processes. In this context, the scale reduction in mechanical fabrication has been permitting the miniaturization of thermal devices, such as in the case of micro-heat exchangers [1]. Recent review works [2, 3] have pointed out discrepancies between experimental results and classical correlation predictions of heat transfer coefficients in micro-channels. Such deviations have been stimulating theoretical research efforts towards a better agreement between experiments and simulations, through the incorporation of different effects that are either typically present in micro-scale heat transfer or are effects that are normally disregarded at the macro-scale and might have been erroneously not accounted for in micro-channels. According to recent statistics, a large proportion of field failures can be attributed to overheating, which in turn is caused by inappropriate thermal design. Uneven thermal maps and "hot spots" in ICs cause physical stress and reduce reliability.

A number of techniques have been proposed in the literature for chip cooling. Initially Tuckerman and Pease [4] proposed micro channel heat sinks fabricated onto the back of a silicon chip substrate. Later on, other means were employed to cool the chips by: immersing the electronic chips in a pool of inert dielectric liquid [5], thermosyphons, where a liquid evaporates with applied heat and condenses dissipating that heat elsewhere, in a closed system [6], and heat pipes, where the liquid evaporates, condenses at another region and reaches the hot area through wick structures that line the heat pipes thus ensuring uniform distribution of heat [7]. These techniques are inherently unsuitable for compact, embedded systems. Thus, there remains a technology void and a pressing need for dynamically cooling hot spots in embedded ICs and compact packages used for portable applications. A wide range of research has been carried out on different processes and application. For instance, Kang and Tseng [8] developed a theoretical model for predicting the thermal and fluid characteristics of a cross flow micro-heat exchanger. In micro-structured devices, homogeneity of the fluid is very important. Tomonomura et al. [9] designed a micro device using CFD. The simulation illustrates that the uniformity of flow greatly depends on the geometry of the shape of micro channels. The present research effort was related to the fundamental analysis of flow behavior and forced convection within micro-channels.

2. Design Details

To determine the best fluid distribution in terms of homogeneity of fluid flow in each of the parallel channels, various geometries were evaluated and studied and the best four convenient ones are stated here.

2.1. Physical description

The basic difference among the four proposed geometries was in the inlet and outlet shapes. Type-01 geometry has a side entrance and a triangular shaped fluid distribution (see Fig. 1(a)). In Type-02, the fluid inflow was in the central part and the distribution was also triangular. In the third proposal (Type-03), the distribution is of convex shape and central inflow. Type-04 geometry is of concave shape. All the inlet geometries are shown in Fig. 1.

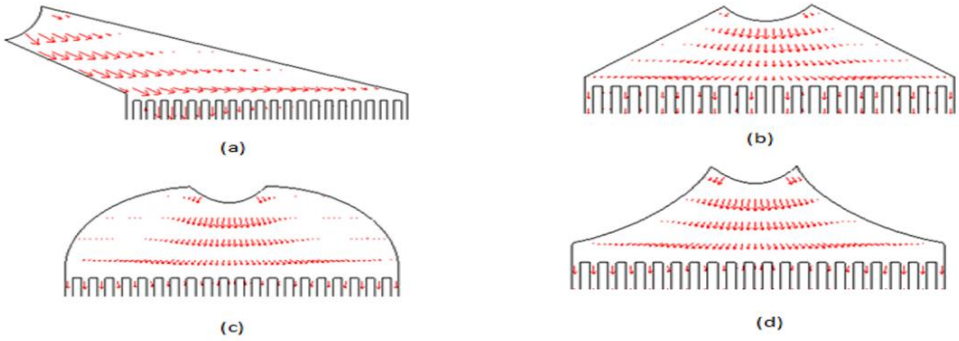

Fig.1. Inlet shapes of different fluid distribution geometry (a) Type-01; (b) Type-02; (c) Type-03; (d) Type-04

2.2. Boundary condition

The flow simulations were done for fully developed inflow velocity, no slip flow at channel walls and zero relative pressure, no viscous stress at outlet.

For temperature distribution, the boundary conditions were constant inlet temperature, constant heat flux at channel wall and convective flux condition at outlet.

3. Computational Procedure

3.1. Mathematical formulation

The basic mathematical equations in determining the flow behavior through the micro-channel are Navier-Stokes equation for momentum conservation and continuity equation for mass conservation.

$$\rho\frac{\partial u}{\partial t} + \rho u.\nabla u = -\nabla p + \mu\nabla^2 u - \rho g \tag{1}$$

$$\nabla.u = 0 \tag{2}$$

For getting temperature distribution, law of convection and conduction for energy conservation was used.

$$\nabla.(-k\nabla T) = Q - \rho C_p u.\nabla T \tag{3}$$

3.2. Assumptions

In the present work, there were some assumptions made for simplifying the problem. The assumptions taken were:

- Fluid flow (M=0.04) was incompressible.
- Fluid was considered as continuum (Kn < 0.01)
- The flow regime was laminar.

4. Simulation

The proposed geometries were simulated under the mathematical model which is governed by the coupled equations of continuity, momentum and energy and was solved by employing non symmetric pattern multi frontal finite element method. For the simulation purpose, Nitrogen and Hydrogen gas of inlet average velocity of 10 m/s was considered. The channel wall heat flux was taken as constant 10000 W/m^2 and the inlet temperature of the gas was taken 300 K.

The coupled governing equations are transformed into sets of algebraic equations using finite element method to reduce the continuum domain into discrete triangular domains. The system of algebraic equations is solved by iteration technique. The solution process is iterated until the subsequent convergence condition is satisfied:

$\left|\Gamma^{m+1} - \Gamma^{m}\right| \le 10^{-6}$ where n is number of iteration and Γ is the general dependent variable.

4.1. Grid independence test

Several grid size sensitivity tests were conducted on Type-03 to determine the sufficiency of the mesh scheme and to ensure that the solutions were grid independent. The test was done with eleven different number of mesh elements. It was found that 111000 non regular elements were sufficient to provide accurate results.

4.2. Code validation

The present results were validated based on the problem of Vasquez-Alvarez et al. [12]. Some of the present results were compared with those reported in Vasquez-Alvarez et al. [12]. The comparison of the average velocity has been shown in Table 1. The present results have a very good agreement with the results obtained by Vasquez-Alvarez et al. [12].

Table 1. Code validation for Type-01

Channel no	Average velocity(m/s)	
	present	reference
1	2.34	2.3
5	2.50	2.45
10	2.61	2.6
11	2.63	2.65
20	2.83	2.7

5. Simulated Figures

5.1. 2-D simulations

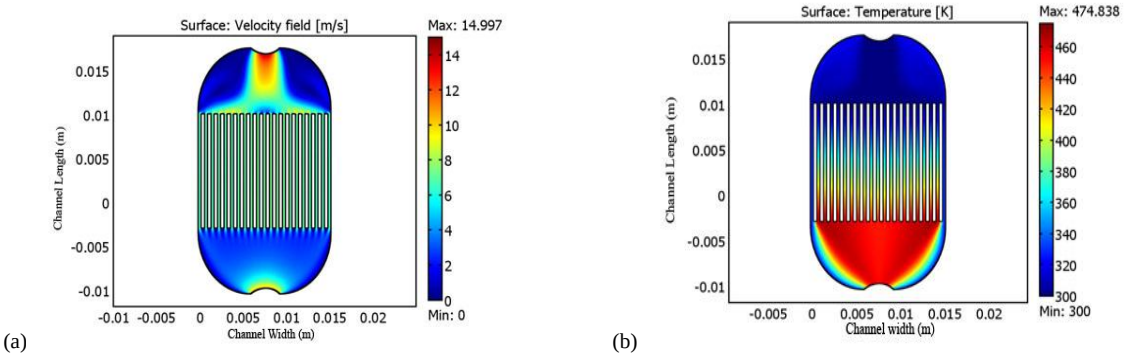

(a) (b)

Fig. 2. (a) Velocity distribution of Type-03 geometry; (b) Temperature distribution of Type-03 geometry

5.2. 3-D simulations

The Type-03 geometry is simulated for Hydrogen in 3-D at 400 Pa inlet pressure. The velocity and temperature distributions are shown in Fig. 3. The units of the geometry are in meter in figure 3.

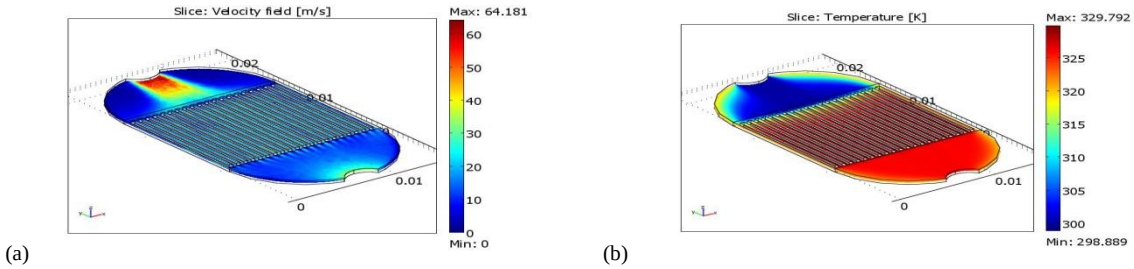

(a) (b)

Fig. 3. (a) Velocity distribution of Type-03 geometry; (b) Temperature distribution of Type-03 geometry

6. Results and Discussion

The proposed geometries were simulated using Nitrogen and Hydrogen as working fluid. The results found have been compared in figure 4 to figure 6.

(a)

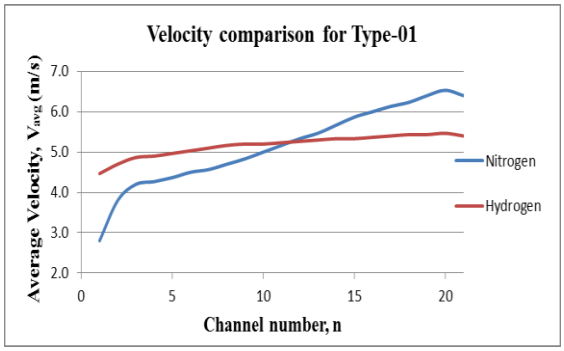

(b)

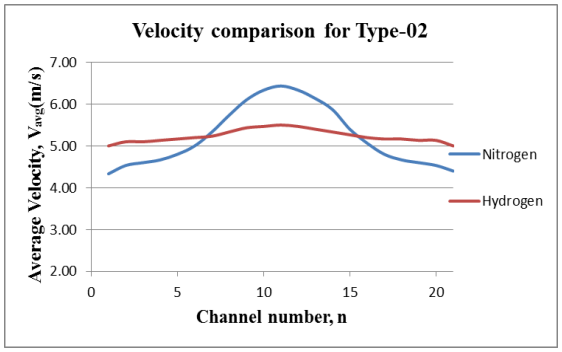

(c)

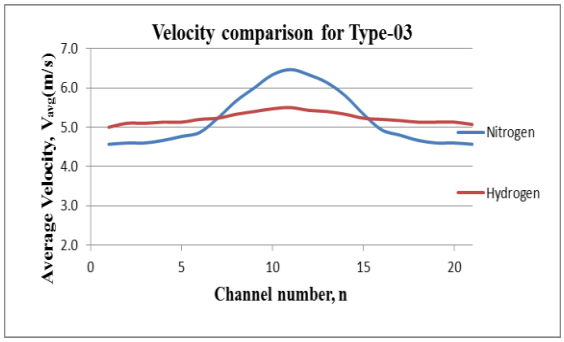

(d)

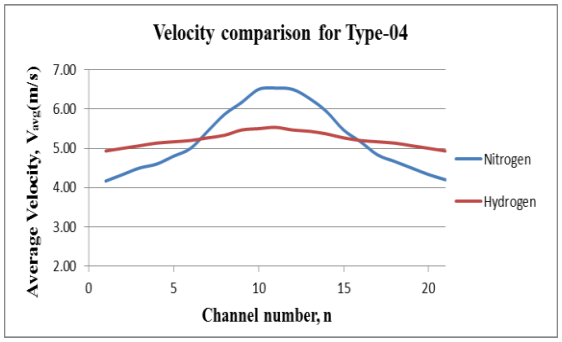

(e)

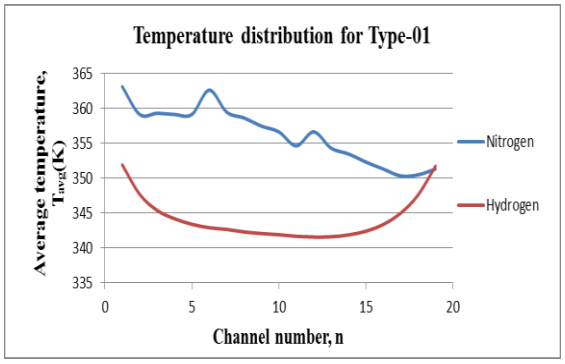

(f)

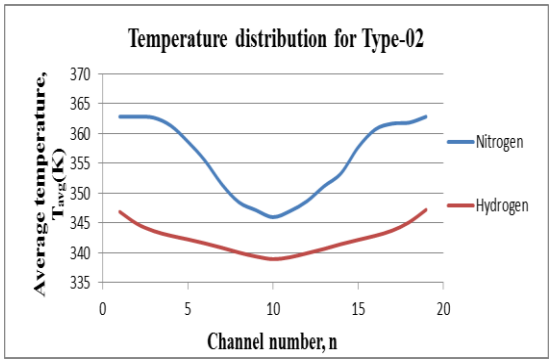

Fig. 4. Velocity comparison for (a) Type-01; (b) Type-02; (c) Type-03; (d) Type-04; Temperature comparison for (e) Type-01; (f) Type-02

(a)

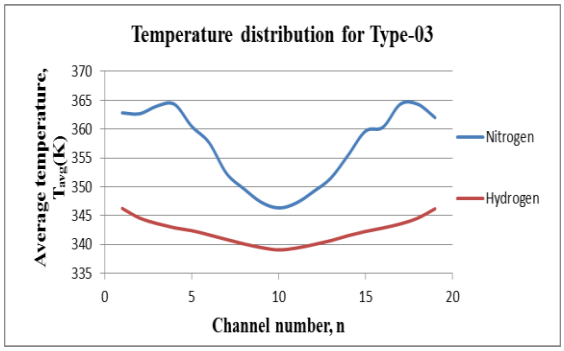

(b)

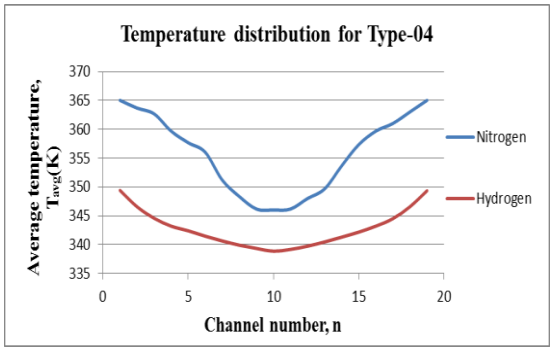

Fig. 5. Temperature comparison for (a) Type-03; (b) Type-04

The results were taken at mid-length of each channel. It is evident from figure 4 and figure 5 that Hydrogen gave more uniform flow than nitrogen and also the temperature was lower among channels for hydrogen. So, velocity and temperature were compared for hydrogen in different geometries in figure 6.

(a)

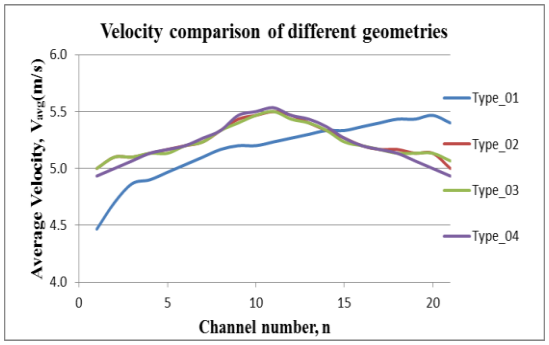

(b)

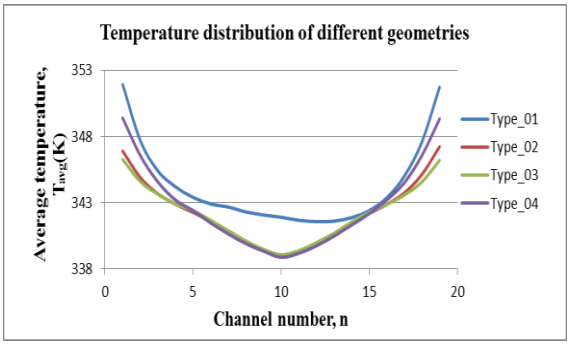

Fig. 6. (a) Velocity comparison for Hydrogen; (b) Temperature comparison for Hydrogen

Except type-01, all the other three geometries gave almost same distribution (Fig. 6). However, distribution for Type-03 is most uniform. So, Type-03 was simulated in 3D for Hydrogen at inlet pressure of 400 Pa. For comparison Type-03 geometry was also simulated in 2D for same inlet pressure. The results obtained are given in Table 2.

Table 2: Velocity Distribution results

Parameters	Unit	2-D							
		Nitrogen				Hydrogen			
		Type-01	Type-02	Type-03	Type-04	Type-01	Type-02	Type-03	Type-04
V_{max}	m/s	15.18	15.00	14.98	15.00	15.21	15.00	15.00	15.00
Re_{max}	Dimensionless	82.4	83.63	167.19	79.89	14.07	14.29	13.35	13.88
ΔP	Pa	242.24	223.20	223.88	229.87	71.79	69.88	69.86	70.85
T_{max}	K	529.96	530.11	531.38	536.83	484.29	474.57	474.83	476.69
				2-D				3-D	
		V_{max}	Re_{max}	ΔP	T_{max}	V_{max}	Re_{max}	ΔP	T_{max}
Hydrogen		67.12	89.70	400	342.5	64.18	522	400	330

7. Conclusion

The computational investigations of flow and thermal fields and heat transfer behaviors in a micro channel heat exchanger have been presented in this study. The channel walls were at constant heat flux of 10000 W/m^2. Inlet fluid temperature was 300K. The results varied greatly with the working fluid and also with the geometries. After simulation process, velocity field, pressure difference, temperature distribution etc were analyzed for solutions of current field problems. Four geometries were analyzed and Reynolds number, pressure difference, maximum temperature etc. were obtained. Except Type-01, all other three geometries gave almost same results. So, any geometry of the three can be chosen depending on the embedding surface and manufacturing flexibility.

It was found from the research that hydrogen gives better performance in all respects. Homogeneous flow distribution, less pumping work, low temperature rise in channels all these are obtained using Hydrogen as working fluid. Later on Hydrogen was simulated in 3D and compared with 2D. The results found from 2D and 3D were almost identical. There is scope for improvement by considering two phase flows in 2D and 3D simulations.

References

[1] C.B. Sobhan and G.P. Peterson, 2008. Microscale and Nanoscale Heat Transfer: Fundamentals and Engineering Applications, CRC Press, Boca Raton.

[2] Yener, S. Kakaç, M. Avelino, and T. Okutucu, 2005. Single-phase Forced Convection in Micro- channels –a State-of-the-art Review, in: S. Kakaç, L.L. Vasiliev, Y. Bayazitoglu, Y. Yener (Eds.), Microscale Heat Transfer Fundamentals and Applications, NATO ASI Series, Kluwer Academic Publishers, The Netherlands, p. 1–24 (2005).

[3] G.L. Morini, 2004. Single-Phase Convective Heat Transfer in Micro channels: a Review of Experimental Results, Int. J. of Thermal Sciences 43, p. 631–651.

[4] D.B. Tuckerman and R.F.W. Pease, 1981. High Performance heat sinking for VLSI, IEEE Electron Devices Letters 2, p. 126-129.

[5] A.E. Bergles and A. Bar-Cohen, 1990. Direct liquid cooling of microelectronic components, In Adv. in thermal modeling of electronic components and systems, 2, p. 241-250.

[6] S.S. Murthy, et al., 2000. "Single chamber compact thermosyphons with micro-fabricated components," Intersociety Conf. Thermal and Thermomechanical Phenomena in Electronic Systems, pp. 321-327.

[7] H. Xie et al., 1998. "The use of heat pipes in personal computers," Intersociety Conf. Thermal and Thermomechanical Phenomena in Electronic Systems, pp. 442-448.

[8] Kang, S-W., Tseng, S-C., 2007. Analysis of effectiveness and pressure drop in a micro cross-flow heat exchanger, Applied Thermal Engineering 27, p. 877-885.

[9] Tonomura, O., Tanaka, S., Noda, M., Kano, M.Hasebe, S., Hashimoto, I., 2004. CFD-based optimal design of manifold in plate-fin microdevices. Chemical Engineering Journal 101, p. 397-402.

[10] Commenge, J-M., Falk, L., Corriou, J-P., Matlosz, M., 2002. Optimal Design for flow uniformity in Microchannel Reactors. AICHE Journal 48, No 2, p. 345-358.

[11] Kockmann, N., 2008. Transport Phenomena in Micro Process Engineering, Springer, Germany.

[12] E. Vasquez-Alvarez, F.T. Degasperi,L.G. Morita,M.R. Gongora-Rubio and R. Giudici, 2010. Development of a micro-heat exchanger with stacked plates using LTCC technology, Brazilian Journal of Chemical Engineering 27 No.3, p. 483-497.